POLITECNICO DI MILANO

School of Information Engineering

Master of Science in
Telecommunications engineering

Electronic, Information and Bioengineering Department

SAR back-projection focusing algorithm with a sub-apertures technique

Supervisor: Prof. Prati Claudio Maria

Graduation thesis of:

Davide Di Nardo

ID: 787111

Academic year 2014-2015

To my family

Acknowledgment

I'd like to thank my family, my friends and my girlfriend that always support me during this study years.
I'd like to thank professor Prati for the help he gives me for all the duration of this work.

Introduction

Synthetic aperture radar (**SAR**) is a general method for generating high-resolution radar maps from low-resolution aperture data which is based on using the relative motion between the radar antenna and the image scene. A synthetic aperture is formed using electromagnetic signals from a physical aperture located at different space-time position. SAR can be seen as a particular case of side-looking radar in which the angular resolution is inversely proportional to the aperture size so that the spatial resolution degrades increasing the distance from the scene. Synthetic aperture is obtained combining the data from the real antenna of a side-looking real-aperture radar as we sample data of a bigger real antenna with size equal to the real-antenna footprint . In this way SAR can observe the scene over a large angular sector by moving the physical aperture to achieve a better resolution in the along-track direction with results that are independent from the range to the scene. The resolution of these system are limited by antenna illumination and system bandwidth but also by other factors, e.g. accuracy of the antenna positioning, propagation perturbation, transmitted power, etc. The ultimate limit of SAR spatial resolution is proportional to the wavelength. Signal processing play a key role in SAR because it is necessary to process all the reiceved echo for all the positions of the synethic aperture in order to obtain the final image and this is why there are many different algorithms of focusing. There are two foundamental features in the focusing algorithms: resolution and computational efficiency. Most of computationally efficient algorithms work in the Frequency-domain such as the Rectangular format algorithm or thet Fourier-Hankel and range migration inversion method. A major shortcoming of the algorithms, however, is that they are derived for a linear aperture and they are not easily extendible to the common nonlinear case. It is possible to partly correct for nonlinear motion, i.e. deviation from a linear track, but the image must be cut into subimages and processed separately since the motion correction is only locally valid. This problem becomes a major issue in wide-beam system e.g. low-frequency SAR where a wide beam is necessary to obtain an acceptable along-track resolution. There is cleary need for other processing algorithms which can be more easily adapted to a general aperture geometry, and this leads to the image formation in the time-domain. A way to consider such an algorithm is the *back-projection integral* used in tomography. In the direct back-projection method, each received radar echo

is processed and back-projected over spherical shells to all imaged ground pixels. Each pixel is thus assigned a value by interpolating the pulse echo at the time delay corresponding to the range beetwen the pixel and the antenna. The value for each pixel is accumulated as more radar echoes are processed and the final resolution achieved. The main drawback of the direct back-projection algorithm is the large number of required operations that are proportional to N^3 for an image with $N * N$ pixel and N aperture positions, since every aperture position must be examined for every image pixel. The purpose of this thesys is to implement a direct-back projection integral partitioning the integral in sub-integrals each correspoding a *sub-aperture*. We divided the syntethic aperture in sub-apertures and then we undersample each of them to increse the algorithm's performance in term of computational cost. The work presented here is structured as follows:

Chapter 1 In this chapter we talk about the generical SAR system and its most important parameters related to the acquisition and focusing problem.

Chapter 2 Here we introduce the acquisition for SAR system in case of linear trajectory and then we extend the problem to the nonlinear case. We also talk about the frequency components of the raw data

Chapter 3 This chapter talk about the back-projection focusing method. We introduce the common continuos time method and then we analyze the use of the sub-apertures.

Chapter 4 After the previous chapters analysis, now we explain our implementation of the sub-apertures back-projetion algorithm introducing the subsample stage to obtain the computational efficiency respect to the common back-projection algoritmh.

Chapter 5 This is the last chapter, here we want study the performance of the algorithm and we find a bound in the subsampling stage that guarantees good results and low phase errors.

Contents

List of Figures

List of Tables

Chapter 1

SAR Fundamentals

In the following we introduce basic concepts relative to Synthetic Aperture Radar (SAR). First we introduce the geometry of the acquisition problem with the assumption that the sensor flight path is a straight line and then we introduce the non linear track motion that, in term of SAR, can be seen as a phase delay in the received signal. In order to analyze the characteristics and properties of the backscattered signal and received onboard, we consider an elementary scene consisting of a single scatterer without loss in generality.

1.1 SAR System

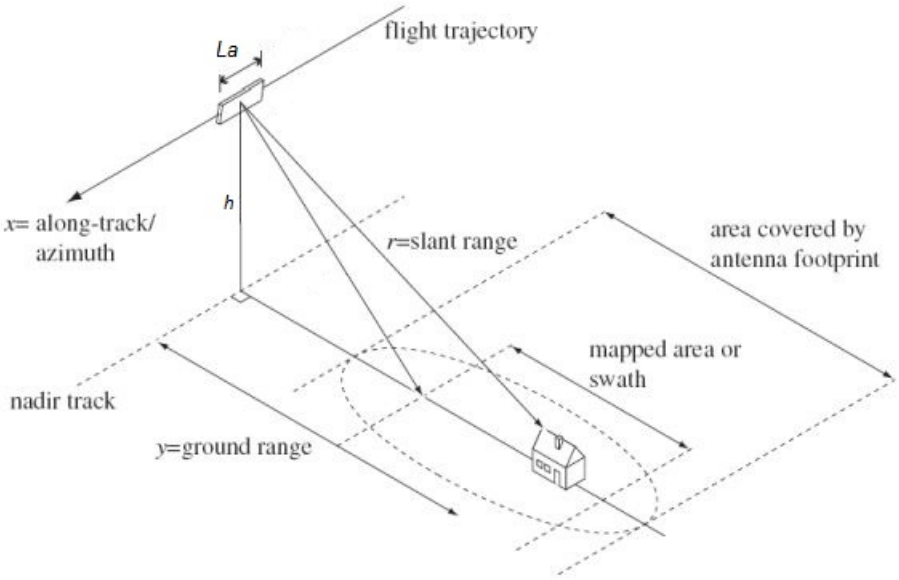

Figure 1.1: Sar system geometry

Consider a radar which trasmits pulses from an antenna with little directivity and receives the back scattered echoes as a function of delay time. Let as refere to figure 1.1, the sensor is moving in the along-track direction $u = x$ with constant velocity v_s and is transmitting pulse $p(t)$ with a constant rate PRF (Pulse Repetition Frequency) that represent the sampling frequency in the azimuth direction. This pulse modulates a carrier signal that is a complex sinuosid with central frequency equal to $f_0 = \frac{\omega_0}{2\pi}$, so the trasmitted signal is

$$s_T = p(t)e^{j\omega t}$$

The way to transmit such signal is to use an IQ modulator and consequently an IQ demodulator to receive the pulses scattered by the targets. As the sensor is mounted over a plane or satellite usually there's a single antenna used both to transmit and receive so we need to switch the real antenna for the two phases. This can be made introducing a system that switchs the circuit for transmission when the time is an integer multiple of the TRI and put the system in "listening" for the other time. In this way we have a **monostatic** radar in which the transmitter and the receiver are positioned in the same location. The scheme of such

system is shown in figure 1.2 while the scheme of a generic IQ system is shown in figure 1.3.

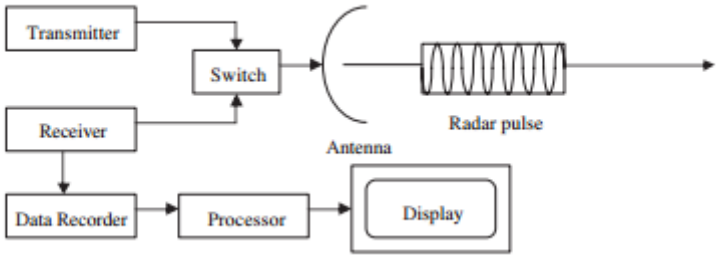

Figure 1.2: Basic block diagram of typical radar system.

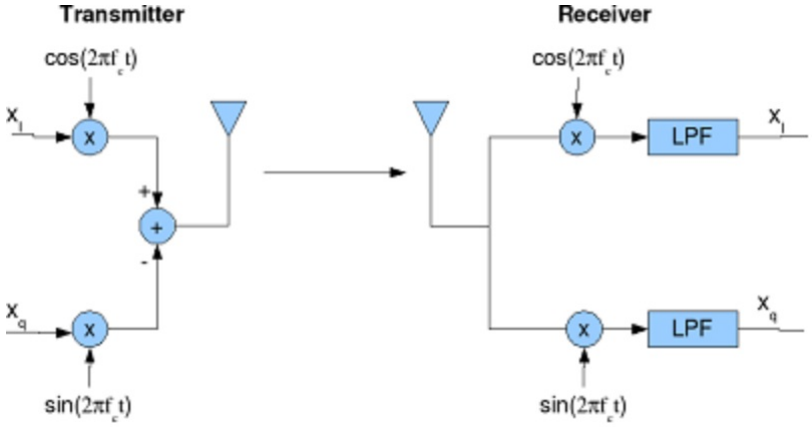

Figure 1.3: IQ modulator-demodulator, x_i and x_q are the components of the complex envelope of the generic trasmitted pulse

1.2 SAR Resolution

The target resolution of a radar is its ability to distinguish between targets that are very close in either range or azimuth. With SAR we reconstruct images in 2 dimensions so we have a resolution for dimension, called azimuth resolution and range resolution.

Range Is the dimension in the line-of-sight of the radar and range resolution is the capability to resolve two close target in this direction. It depends on

the bandwidth of the transmitted pulse, just as in digital communication we say that the bandwidth of a signal is approximately inverse to the time duration. In fact we can resolve two close targets if the pulsed echoes are not overlapped in time, so we obtain:

$$\rho_r = \frac{c}{2B_p} \tag{1.1}$$

The factor 2 in the denominator is due to the two way path travel of the signal.

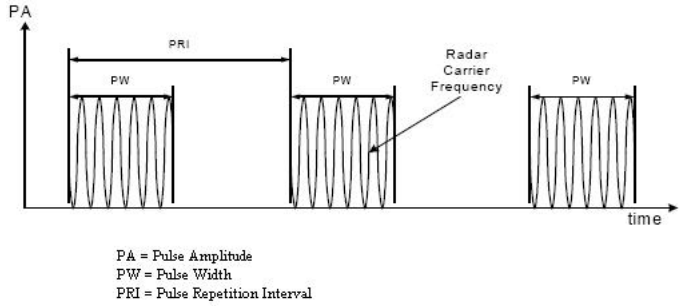

Figure 1.4: trasmitted radar pulse over time

Azimuht In SAR radar systems the azimuth resolution is the capability to distinguish targets that are close in azimuth, that is the moving direction of the sensor. Like in real-aperture radar this resolution is governed by the antenna but in SAR we synthesize a longer antenna through the sampling of the real one. Starting from the theory of the antenna array we can demostrate that the synthetic aperture is equal in length to the footprint of the real antenna [1]. In fact we have to combine all the correlated samples togheter to obtain a finer resolution. We start from the azimuth resolution for a real-aperture radar; it depends on the range R and on the aperture angle.

$$\Delta\psi = \frac{\lambda}{L_a}$$

Adding the formula of the Synthetic aperture

$$L_s = R_0 \frac{\lambda}{L_a} \tag{1.2}$$

instead of the real one and adding a factor 1/2 due to the double travelling of the pulse, we arrive at the well known azimuth resolution formula for SAR systems:

$$\rho_{az} = \frac{L_a}{2} \tag{1.3}$$

where $L_a[m]$ is the azimuth dimension of the real antenna. This is a key formula for SAR because it tells us that to get better resolution we have to decrease the size of the real antenna, i.e. increase the aperture of the real one's angle. The explanation is that the increases of the real azimuth aperture corresponds to increase the synthetic aperture and this is the relation that governs the resolution. An illustration of this is in figure 1.5.

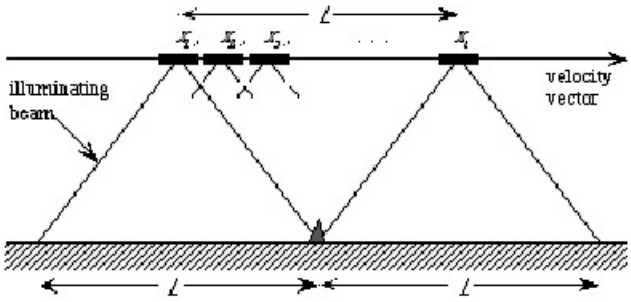

Figure 1.5: Synthetic aperture "on air" is equal to footprint on the ground made by the real antenna; they have the same azimuth length L

1.3 Sampling the Array

Syntethic aperture is equivalent to any antenna array and so a critical factor is the sampling interval. We have to respect the Nyquist criterion to avoid aliasing. First assuming that each antenna limits the DOA within the range

$$-\psi_M < |\psi| < \psi_M$$

Where ψ_M is the maximum real antenna angle aperture. According to equation 1.6

$$\psi_M = \frac{\Delta\psi}{2} = \frac{\lambda}{2L_a}$$

By the linear antenna array theory we know that a spatial frequency corresponds to an angle of view, so we have a maximum spatial frequency

$$f_{xM} = 2\frac{\sin\psi_M}{\lambda}$$

For the Shannon theorem, for a spatial sampling interval dx given we obtain:

$$\frac{1}{d_x} > 2f_{xM} \quad \Rightarrow \quad d_x < \frac{\lambda}{4\sin\psi_M} \tag{1.4}$$

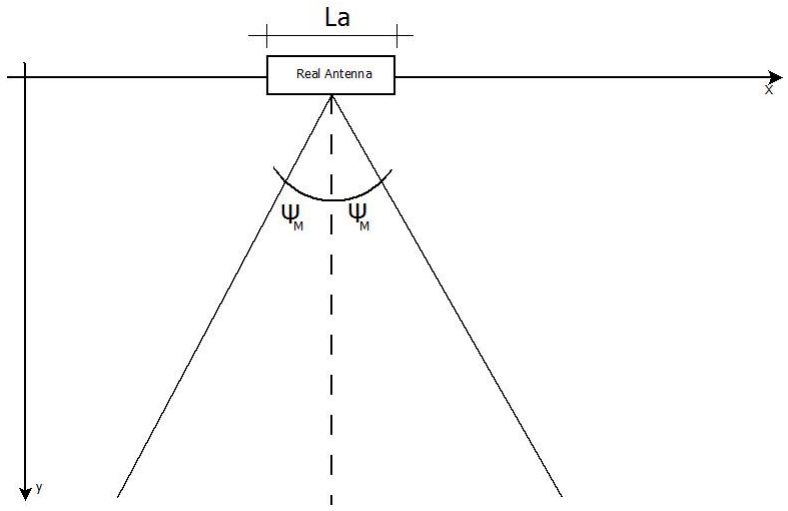

Figure 1.6: Angular aperture for a real antenna of azimuth length L_a

whence the maximum spatial frequency occurs when $\sin\psi_M = 1$ so, sampling for any angular direction, we have:

$$dx = \frac{\lambda}{4}$$

The quantity dx cannot be set as small as we want because

$$dx = v_s \cdot T_{PRI} = \frac{v_s}{f_{PRF}}$$

Form the relation above fixed the platform velocity v_s,dx cannot be set as small as we want becaus it can reduce T_{PRI} to an impossible value so there's need a tradeoff between real angular aperture, synthetic aperture, azimuth resolution and sampling interval.

In equation 1.2 we introduce the syntethic aperture length for a generic SAR system. It is important to observe how much this quantity is related to the aperture length of the real antenna and this governs the SAR azimuth resolution. This concept is the strength of SAR because if we want to get a given resolution we have to fix the size of the real-antenna and from this parameter we get the size of the synthetic aperture.

1.4 Data structure

SAR systems acquire a lot of data during the scan session and these data are stored in memory after the sampling process. The processing stage works on these bins to obtain final images. Data are sampled both in azimuth and range dimensions so we obtain a matrix data structure, i.e. the *raw data matrix*. The columns store the data of the backscattered echoes and each sample is taken with

the range sampling frequency $\frac{1}{dr}$, so the raw index "move" the column and marks the *fast time*, i.e. the coordinate associated to the range direction. On the other hand the column index mark the *slow time* that is the coordinate associated to the azimuth position of any "sensor" of the syntethic array.

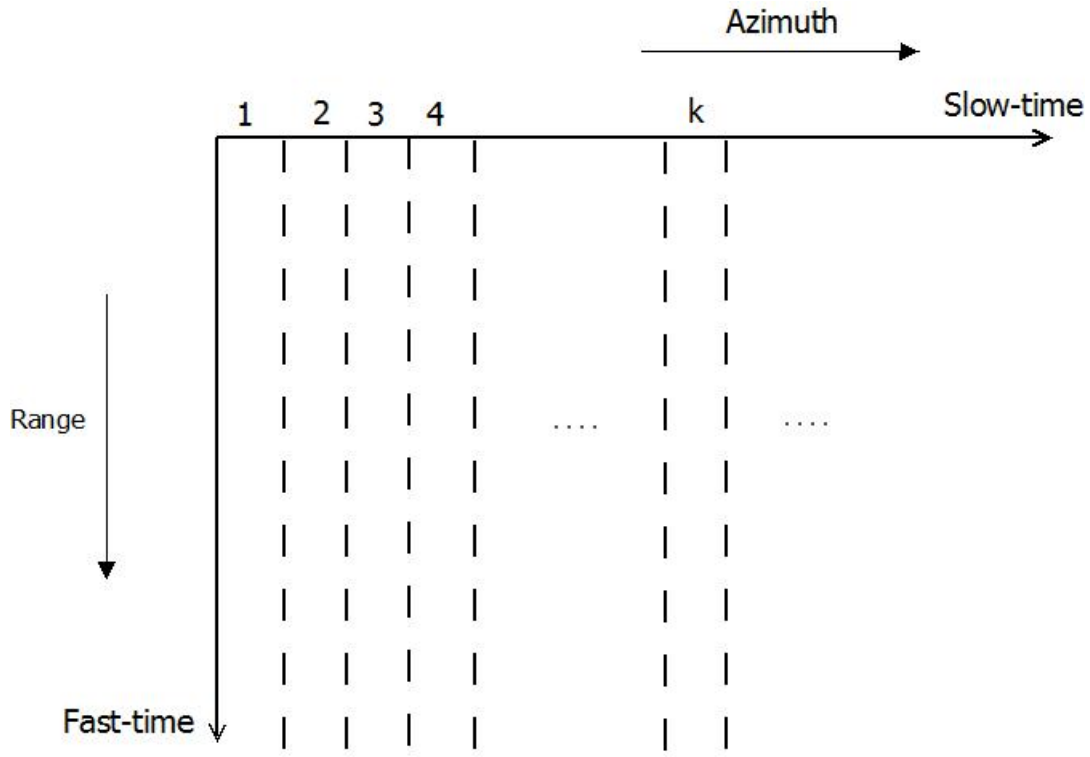

Figure 1.7: Two-dimensional SAR data space.

Chapter 2

SAR Acquisition

In this chapter we talk about the data acquisition in SAR systems. We start from the geometry of the problem using a linear fligth track and then we extend the results to a non-linear motion. This passage is easy because in terms of model it represents an additional phase term. In the following some assumption are made in order to simplify and make clearer the reading but we don't lose in generality. We come to define a IRF (impulse Response function) that enterely describes the SAR acquisition in order to have the tools to make the data focusing.

2.1 RAW DATA

Let us refer to figure 2.1, where the SAR system geometry is depicted, the trasmitted signal is

$$s_T(t) = p(t)e^{j\omega_0 t}$$

where

$p(t)$ is the transmitted pulse; in our simulation $p(t) = sinc(t) * rect(\frac{t}{T_R})$

ω_0 is the central carrier frequency, in the raw data we will demodulate it.

The received signal from a single target positioned at coordinates (x_p, y_p), setting $R_0 = \sqrt{h^2 + y_p^2}$ as the minimum distance sensor-target and assuming that the antenna beam is positioned broadside, is

$$s_r(t, x-x_p, y-y_p, h) = \gamma(x_p, y_p) \cdot p(t - \frac{2R_T(x)}{c}) \cdot w^2(x-x_p, y-y_p) \cdot exp(j\omega_0(t - \frac{2R_T(x)}{c})) \tag{2.1}$$

where:

$\gamma(x_p, y_p)$ is a complex number that accounts both the RCS, the spherical divergence and other attenuations. We put this term equal to $\delta(xp, yp)$, in order to obtain the SAR response for a single point-like target.

$2R_T(x)$ is the double distance beetwen the target and the antenna of the array due to the double path made by the pulse. If a single target is fixed this term depends only on the position $x = u$ of the sensor along the azimuth direction.

$w^2(x - x_p, y - y_p)$ is the illumination fuction of the real antenna, this term depend on the target- sensor positioning too. We assume that the phase center of the radar antenna is located at the coordinate $(h, x = vt, R_0)$

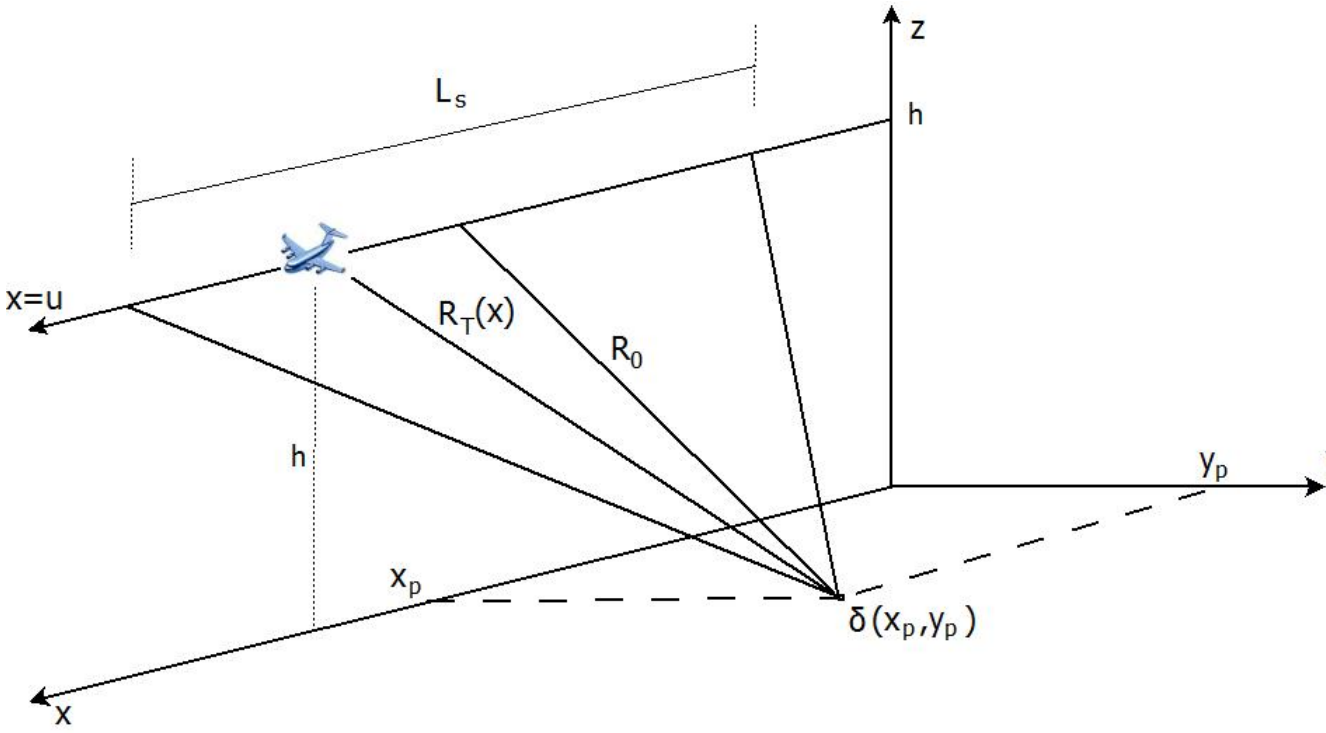

Figure 2.1: Geometry of linear trajectory SAR system.

To obtain the raw data we have to demodulate eq. 2.1 multipling it with a complex exponential $e^{-j\omega_0 t}$. Taken account of the above mentioned approximation and supposed that the *start-and-stop* approssimation applies, i.e. the system is actually *monostatic*; the demodulated received signal is

$$s_r(t, x-x_p, y-y_p, h) = p(t-\frac{2R_T(x)}{c})\cdot w^2(x-x_p, y-y_p)\cdot exp(j\omega_0(\frac{2R_T(x)}{c})) \quad (2.2)$$

Equation 2.2 is a simplified continuous-time version of the *Impulse Respone Function* (IRF) $h(x, t, x-x_p, y-y_p, h)$ for a point-like target $\delta(xp, yp)$. $R_T(x)$ is a very

important variable in SAR, in fact the last term of eq. 2.2 shows that we have a pure phase term that depend on this variable that is called *hodograph*. Moreover we can see that the trasmitted pulse is received with a certain delay that depends exactly from the hodograph. It is a crucial feature in focusing because we have to take the sample at a distance equal to $R_T(x)$. In the picture below an example of a raw data matrix is shown.

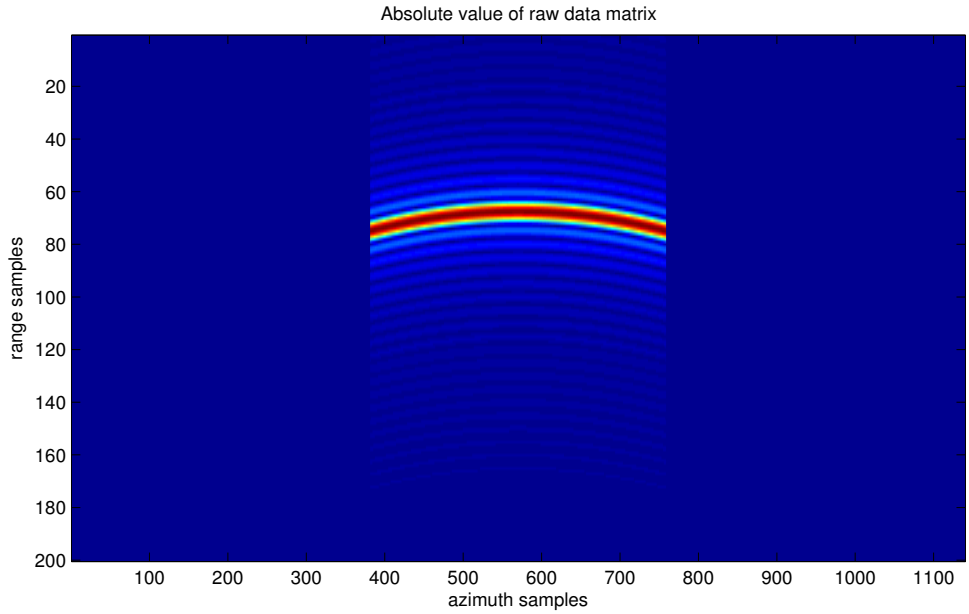

Figure 2.2: Absolute value of raw data matrix for a single point-like target.

2.2 Hodograph and RAW Spectral Analysis

The spectral components of raw signals depend on the geometry acquisition. In fact in equation 2.2 the last term is a pure phase term so it reprsents a complex sinusoid with a space-variant phase. To study this term we start from figure 2.1 and we make a 2D observation of the geometry rembering the assumptions made on the phase center of the antenna. $R_T(x)$ can obtained applying the Pythagoras's theorem according to figure 2.3

$$R_T = R_T(x) = \sqrt{R_0^2 + (x - x_p)^2} = R_0\sqrt{1 + \frac{(x - x_p)^2}{R_0^2}} \tag{2.3}$$

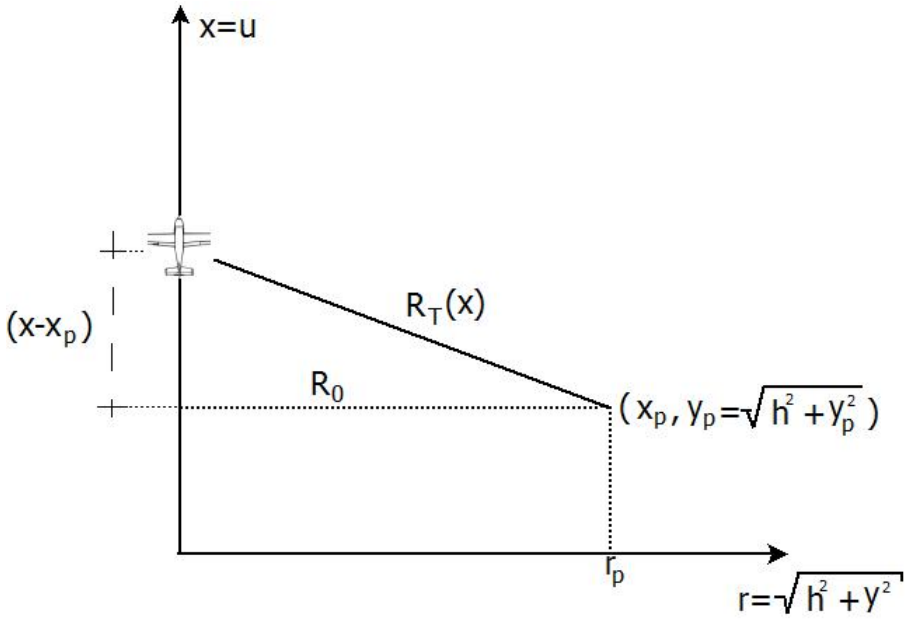

Figure 2.3: 2D geometry of linear trajectory SAR system.

Where R_0 is the *minimum target-sensor distance*; in linear flight track we get this when $x = u = x_p$ and so

$$R_0 = \sqrt{h^2 + y_p^2}$$

where h is the height of the sensor from the ground. Equation 2.3 shows that in a stripmap SAR, the range between the radar and an arbitrary scatter varies hyperbolically as the radar moves along the synthetic aperture. We said that the received pulse has a delay that depends from $R_T(x)$, from eq. 2.3 it is clear that there is an hyperbolic distribution as well. So In the fast-time of the raw matrix we have the same pulse with a certain delay in every column of the matrix, like shown in the picture below.

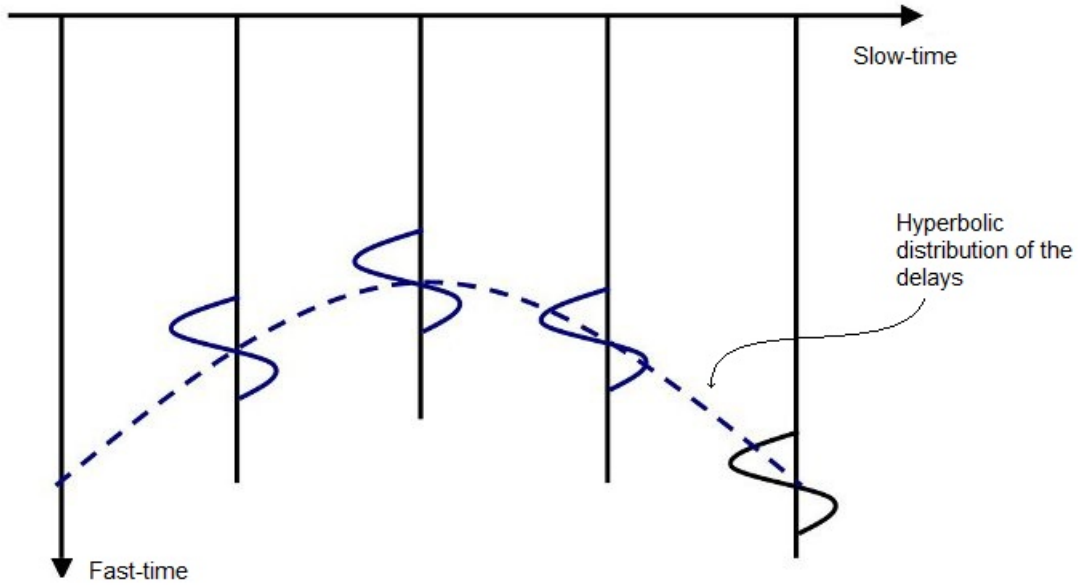

Figure 2.4: Hyperbolic distribution of the delays in the slow-time.

The form of the range variation is invariant to the scatterer's along-track position x_p, in the sense that the x_p dependence of R_T involves only the position of the aircraft relative to the scatter, $(u - x_p)$, but, in contrast, the range variation varies with the absolute slant range of the target, R_0 that depends on position y_p. We now observe that usually the range distance is greater than the distance to the point in the array

$$R_0 \gg (x - x_p)$$

within a synthetic aperture and this is equal to say that the *far-field approximation* applies. After that we can use the Taylor series stopped at the first order for the square root and we obtain:

$$R_T \simeq R_0 + \frac{(x - x_p)^2}{2R_0} = R_0 + \frac{x^2}{2R_0} - \frac{(x - x_p)}{R_0} + \frac{x_p^2}{2R_0} \tag{2.4}$$

Equation 2.4 shows that the range from the radar to the target varies approximately quadratically as the data set is collected, like shown in figure 2.2, in which we have only a slight quadratically trend. If we now put this result of the hodograph in the last term of equation 2.1 we observe that the received phase of the target echo is shifted by an amount *proportional to range*, namely $\phi = \frac{4\pi}{\lambda} R(x)$. It follows that the absolute phase of the received echoes will also vary approximately quadratically. We now derive the istantaneous frequency term corrisponding to

this phase modulation, simply deriving the phase term:

$$K_{xi} = \frac{d\phi(x)}{dx} = \frac{4\pi}{\lambda}\frac{(x - x_p)}{R_0} \qquad [rads/m] \tag{2.5}$$

In the above equation we obtain the istantaneous frequency expressed in term of *wavenumber*, if we want to change in spatial frequency we have to divide by 2π. From equation 2.4 and 2.5 we note that targets at the same range but in different azimuth positions give the same frequency modulation so the raw data have the same spectrum. Another information that we can see from eq. 2.5 is that the azimuth component's frequency of the raw data have a linear trend with slope equal to K_{xi}, so in frequency we get an *azimuth chirp* like shown in figure 2.5.

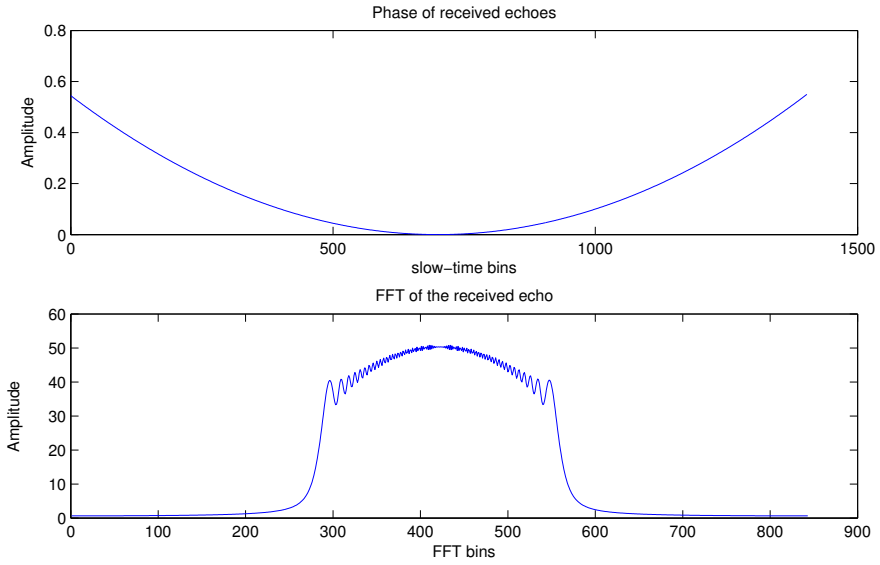

Figure 2.5: Abs of raw and fft signal for a single range and single synthetic aperture.

Note that the curvature in DFT of the raw data in figure 2.5 is due to the illumination function $w(x, r)$ Fourier transform. From eq. 2.5 we can also see that the spectrum components, as we said above, involves only the position of the aircraft relative to the scatter. If we have more scatters in different x-position and at different range positions, but if the range difference is small respect to the the nominal R_0, then they have approximately the same spectrum components, i.e. the same absolute value of their Fourier Transform, like show in figure 2.6.

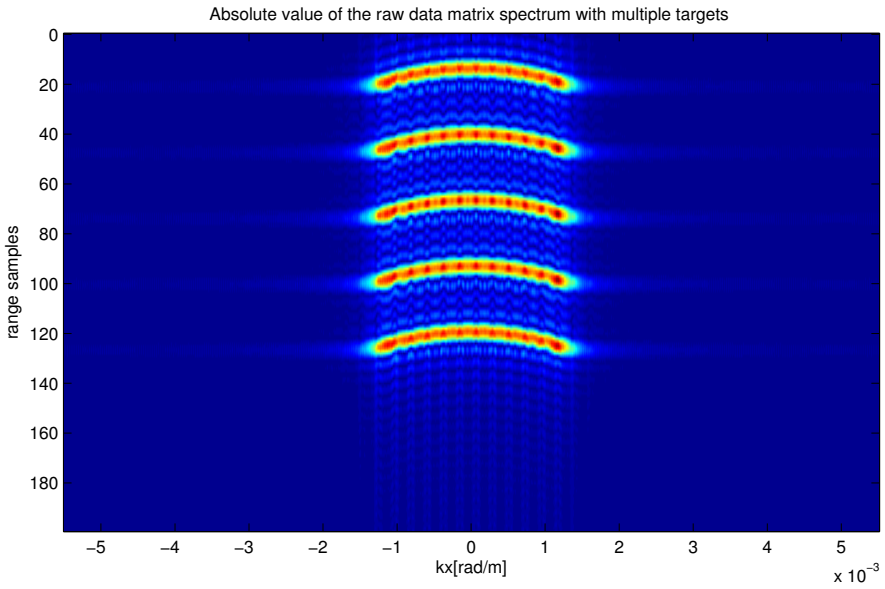

Figure 2.6: Absolute value of the raw FFT with multiple targets, it can be seen that they have approximately the same spectrum.

2.3 RAW data for non-linear trajectory

In case of airborne sensors, significant deviations from the ideal trajectory, due to the presence of atmospheric turbulences may occur, so we want to extend our model in order to describe this effect. The geometry of this case is showned in figure 2.7. Assume that the sensor is moving only on the $z-y$ plane, i.e. now we have $h = h(x), y = y(x)$. To determinate the non linear trajectory effects we have to analize equation 2.3. Said $R_0 = \sqrt{h^2 + y_p^2}$ the nominal target-sensor minimum-distance and said $\Delta r(x) = f(h(x) - h, y(x) - y_p)$ the distance between the nominal sensor trajectory and the actual path, we have:

$$R_{T_{nl}}(x) = \sqrt{(R_0 + \Delta r(x))^2 + (x - x_p)^2} \tag{2.6}$$

2.6 shows that is convenient to rewrite the SAR acquisition expression in terms of plane position x and sensor distance to the target $r = r(x)$ that accounts the deviation from the linear track.

$$\begin{aligned} &s_r(t, x - x_p, y(x) - y_p, h(x)) = s_r(t, x - x_p, r) = \\ &= p(t - \frac{2R_{T_{nl}}(x)}{c}) \cdot w^2(x - x_p, r) \cdot exp(j\omega_0(\frac{2R_{T_{nl}}(x)}{c})) \end{aligned} \tag{2.7}$$

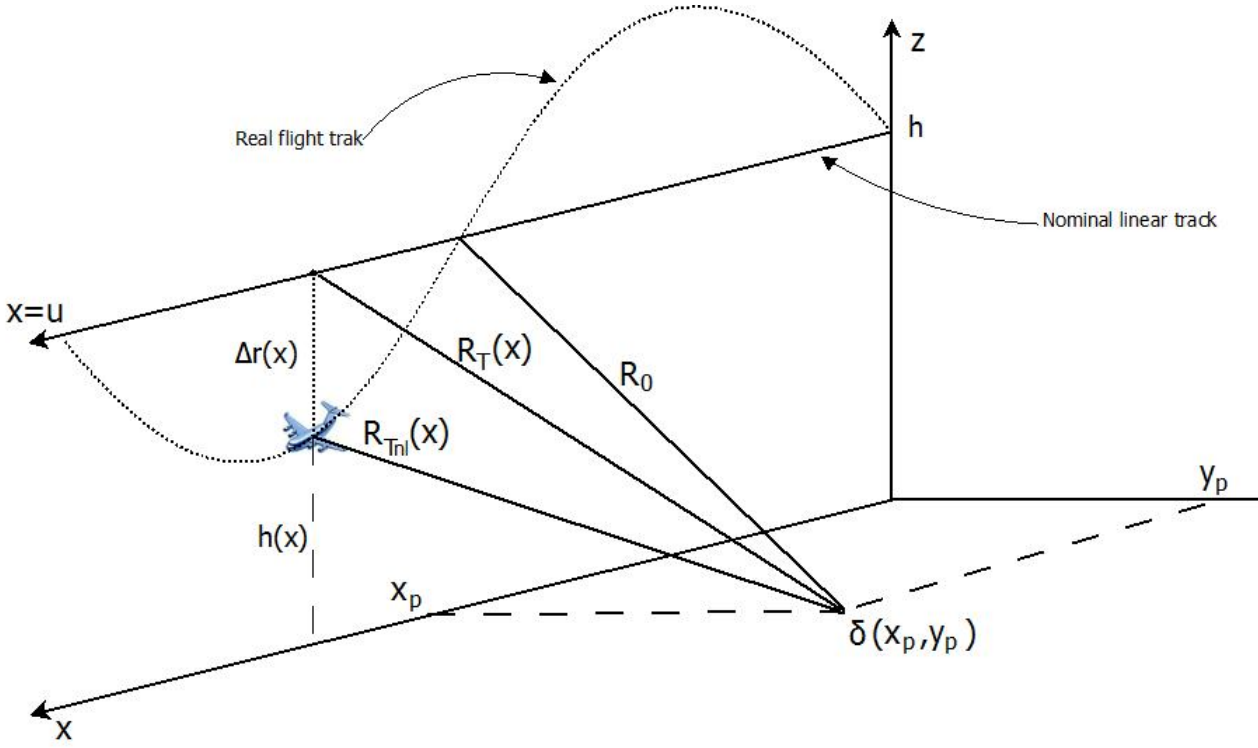

Figure 2.7: Geometry of non linear trajectory SAR system.

Eq. 2.7 is more general than 2.2 and we can use this one to describe the acquisition in all situations. The term $\Delta r(x) = f(h(x) - h, y(x) - y_p)$ can be calculated using the cosine theorem, knowing the angle between the nominal minimum range and the actual x-position of the sensor. Certainly the result expressed in eq. 2.5 will not hold on when the trajectory is non linear, so the spectrum will not be the same as the ideal case. In fact in 2.5 we derive the istantaneus frequency components of the raw signal, and we see that it has an approximate parabolic trend, that depends upon the linear geometry. Now we have a non-linear geometry that modifies the wavenumber component according to

$$K_{xi} = \frac{d\phi(x)}{dx}$$

where

$$\phi = \frac{4\pi}{\lambda} R_{T_{nl}}(x)$$

So now 2.5 doesn't hold on and the closed form of the phase component is more complex because the term $\Delta r(x)$ had a x dependence, so the exactly funtcion of the trajectory has to be known in order to calculate the derivative. The equation above shows that the trajectory modifies the spectrum component of the raw

signal respect to the ideal linear case. In the following two figure the effect of the non-linear trajectory in the raw data spectrum is shown. The same system parameters are used and a single point like target is used.

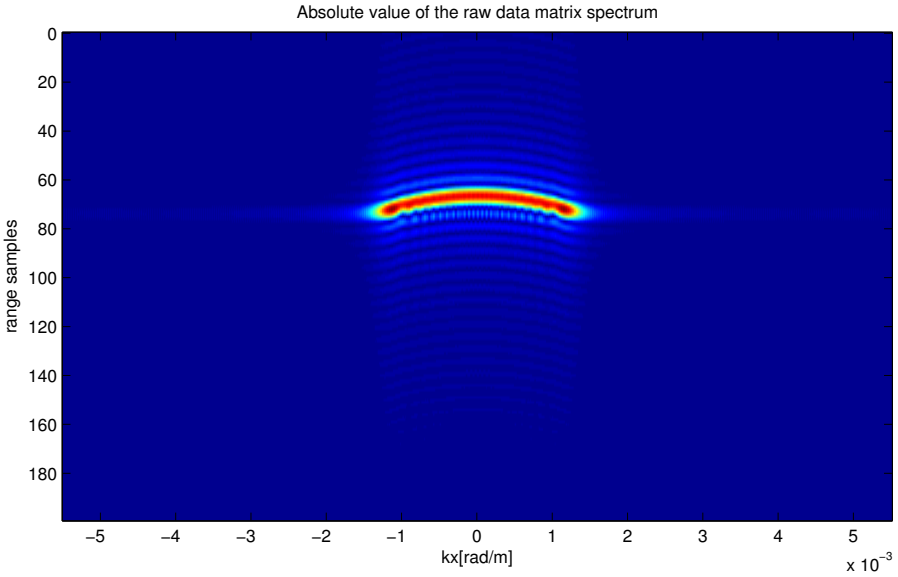

Figure 2.8: Absolute value of a raw signal spectrum for linear trajectory

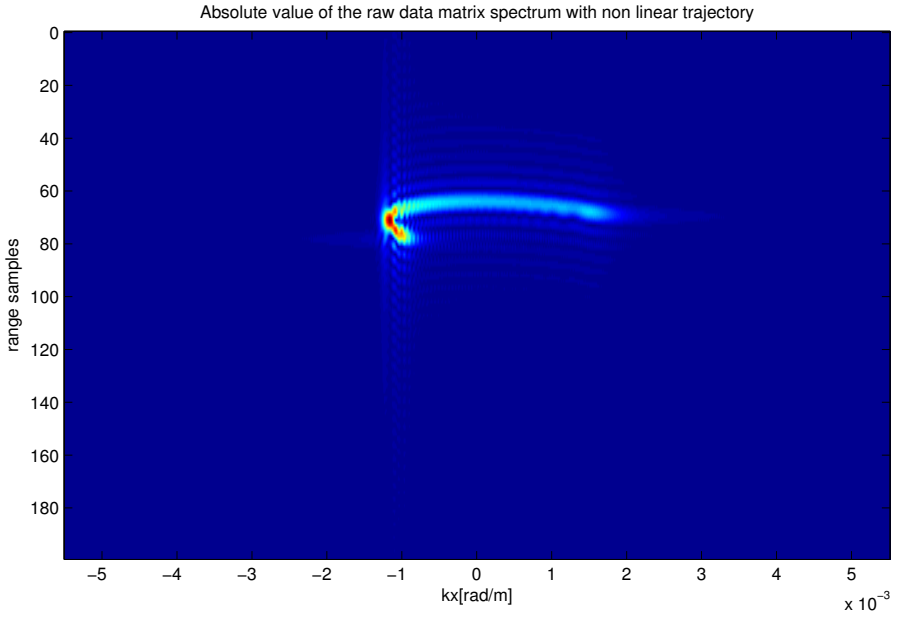

Figure 2.9: Absolute value of a raw signal spectrum for a non-linear sine like trajectory

It can be seen that the spectrum with a non linear trajectory has been modified respect to the linear case. In the next figure we can observe how the raw data matrix changes with a non-linear trajectory, according to equation 2.6. The *hodograph* doesn't have a parabolic trend like shown in figure 2.2 yet but now has also a term due to the non linear track-motion, so from eq. 2.7 the pulse delays don't have a parabolic distribution yet.

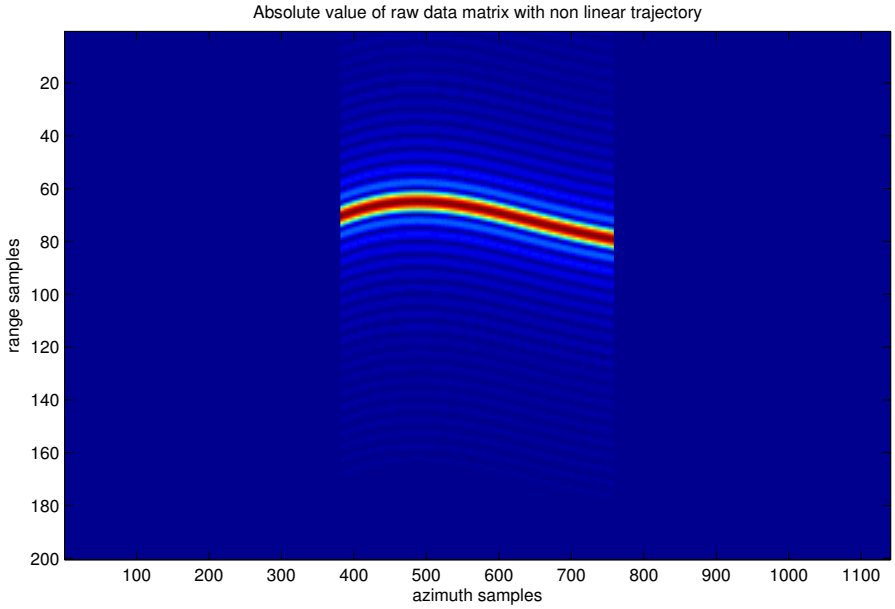

Figure 2.10: Absolute value of a raw data matrix for non-linear sine like trajectory. The effect of the sensor motions can be valued respect to figure 2.2.

Chapter 3

SAR Focusing

The purpose of SAR is the capability to obtain better resolution by sampling a bigger synthetic antenna to form a synthetic array. After the acquisition process and the construction of the raw data some processing stages are required in order to synthesize this antenna and get the higher resolution. The set of operations that we do on the raw data, to obtain the image of the illuminated area, is called *focusing*. Mathematically the focusing is the inversion of the acquisition, represented by equation 2.2. The simpliest focusing method is *the matched filter* of the IRF, that corresponds to the optimal estimation of an isolated target [1]. Although that method is simple and guarantees good results also with non-linear flight tracks, it's very expensive in terms of computational cost as we have to process, for all pixels in the final image, all the relative points in the synthetic aperture. There are a lot of algorithms to speed up the focusing process, usually based on the *Fourier transorm* like the *Range doppler algorithm* and the $\omega - k$ algorithm. In the following we analyze the time-domain method called *back-projection* that corresponds to the matched filter method. We propose an accelerated version of that method dividing and sub-sampling the algorithm in the so called *sub-aperture* in order to decrease the processing burden. We start to talk about the general back-projection method like the inversion problem of the acquisition and then, in the next chapter, we talk about our implementation.

3.1 Time domain focusing method

In eq. 2.7 we derive a continuos-time approximation of the IRF for a single scatter point $\delta(xp, yp)$ with arbitrary flight trajectory. We first introduce the direct problem that is the acquisition, obtained by convolving the above IRF with the reflectivity model of the ground that we are observing. The reflectivity is a continuos or discrete model of the ground; from the point of view of SAR it is a complex function of (x, y) and we call this $a(x, r)$. In this first analysis we suppose to have a continuos function both in azimuth and range. The received

radar signal can be expressed as a convolution between the IRF of 2.7 and the reflectivity model $a(x, r)$:

$$d(x, r) = \iint a(x, r) h_s(t, x, r)\, dx\, dr \tag{3.1}$$

If the scene consists only by a single target the equation 3.1 and 2.7 coincide. To obtain a figure that shows the target on the ground we have to focus the data, so we have to invert eq. 3.1. Focusing defines a trasformation from the raw data to focused data that minimize the distance $\|\hat{a}(x, r) - \hat{a}(x, r)\|$ in some norme. The simpliest solution consist on the use of the *matched filter* that corresponds to the optimum estimation for an isolated target. It is implemented by convolving the raw received signal with a complex conjugate model of the IRF:

$$\hat{a}(x, r) = G(d(x, r)) = \iint d(x, r) \cdot h_s^*(t, x, r)\, dx\, dr \tag{3.2}$$

3.2 is very simple and gives very good results but it is very expensive in term of computational costs, in fact we have to make a linear combination between all the samples of the raw signal and all the points in the final image.

3.2 Back-projection method

We start now to talk about the method we use in this thesys, the back-projection algorithm. The foundamental principle consist on generating a radar map in which each object is located at its 2-parametric position (x, r). The radar map is assumed to be a linear transformation from the radar echo data so that superposition of imaged point object applies. We introduce the back-projected signal $y(x, r)$ as follows:

$$y(x, r) = \int_{-\infty}^{\infty} d(x, r) \cdot h_s^*(t, x, r)\, dx \tag{3.3}$$

For each image position (x, r) the along track integral sums the value from each radar echo at the range corresponding to the distance between the antenna and the image position. It can be demostrated [5] that for a single scattered point located at (x_0, r_0) the back-projected and filtered radar echo data produces a Dirac-function located at (x_0, r_0). Since superposition applies we may add an arbitrary number of point objects at different location and with different amplitudes and still have the exact scene inversion. In our case we work with sampled signal, so we now derive the back-projected signal of equation 3.3 in a discrete time way. To do that we first have to change the coordinates in time-azimuth to the coordinates that we use in the raw data matrix, that are the slow-time, fast-time. Given the sampling period both in range(time) and azimuth called respectively dr and dx we get the discrete time variables of the two quantities:

$$nr = \frac{ct}{2} * dr \quad , \quad na = x * dx \tag{3.4}$$

The expression above transforms the time-azimuth coordinates to the fast and slow time coordinates that are those used in the raw data matrix. Putting these discrete indices in equation 2.7 we get

$$s_r(nr, na - x_p, r) = p(nr - \frac{2R_{T_{nl}}(na)}{c}) \cdot w^2(na - x_p, r) \cdot exp(j\omega_0(\frac{2R_{T_{nl}}(na)}{c})) \quad (3.5)$$

that is the discrete version of the received signal, so it is the signal stored in the raw data. Now we can rewrite the formula of the back-projection integral in the discrete time case as

$$y(na, nr) = \sum_{k=-\infty}^{+\infty} d(na + k, nr) \cdot h_s^*(nr, na + k, r) \quad (3.6)$$

where r is the distance between the pixel that we want to focus and the sensor azimuth position equal to $na + k$. Formula 3.6 has to be applied for every image points (na, nr), with

$$na \in [-N/2, N/2] \quad and \quad nr \in [-M/2, M/2] \quad (3.7)$$

In the real case we don't have to move all samples in the slow-time k as the illumination fuction of the antenna $w^2(na - xp, r)$ bounds the samples that are correlated to those that we want to focus. The number of samples that we have to process is exactly the synthetic aperture length multipled by the sampling interval.

$$k \in [-\frac{L_s}{2}dx, \frac{L_s}{2}dx]$$

Next figure illustrates the logical mechanism made by eq. 3.6 to get a focused pixel at a generic position (na, nr) in the final image.

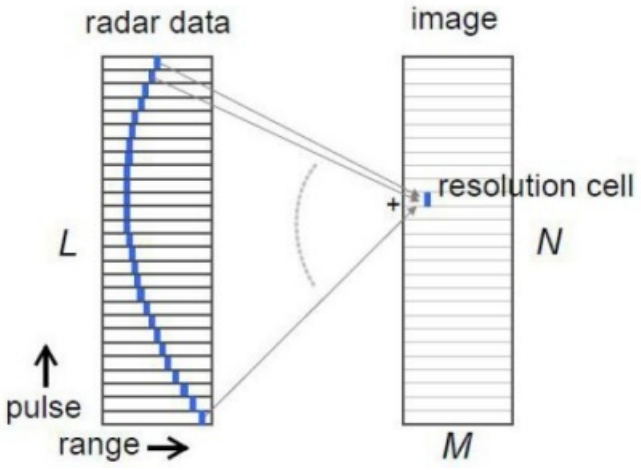

Figure 3.1: Illustration on how the BPI integrates the contributing aperture position to create one image position

The next two figures show instead how a focused point-like target and its spectrum appears .

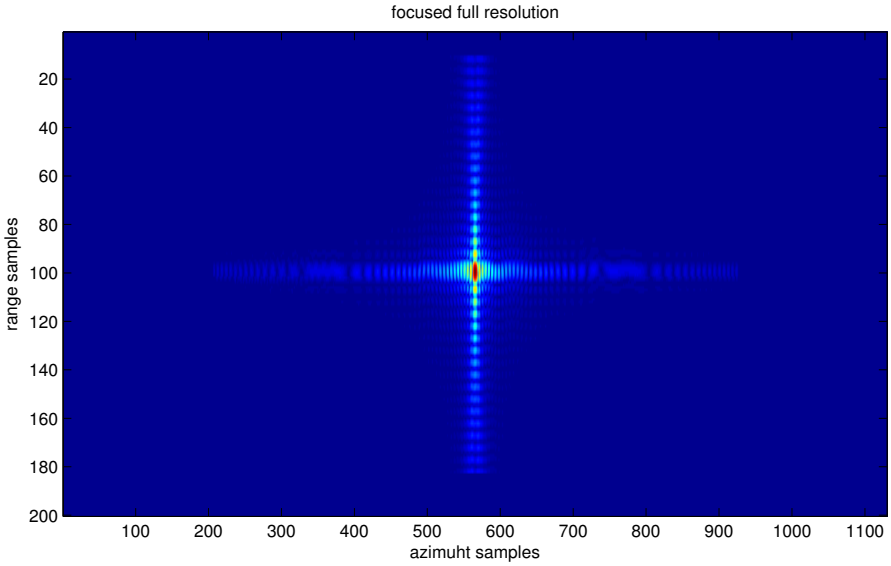

Figure 3.2: Focused final image for a point like target positioned at the center of the image

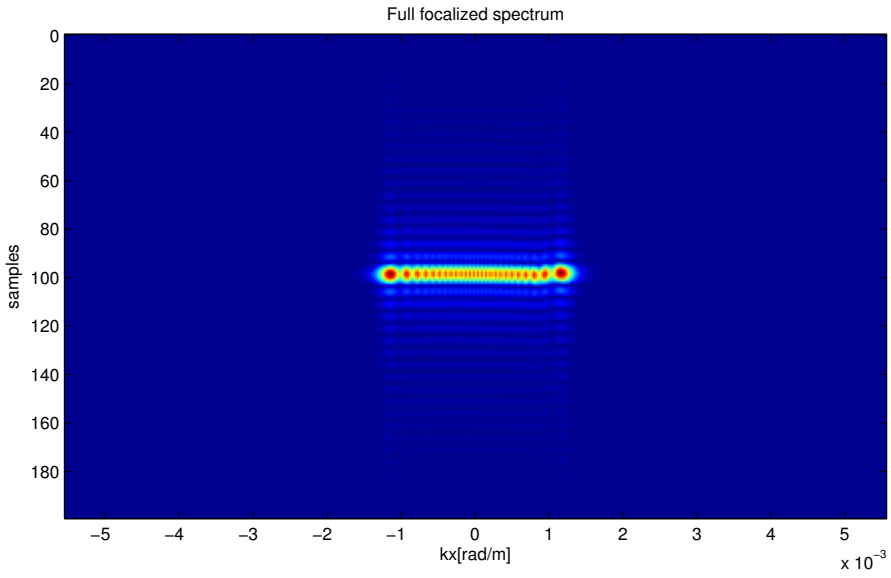

Figure 3.3: Focused spectrum for a point like target positioned at the center of the image

3.3 Sub Aperture back projection integral

The first step to implement our algorithm is to divide a single synthetic aperture in more sub-apertures. If we want to get S sub-apertures we have to divide the expression 1.2 as:

$$L_{s_{sub}} = \frac{L_s}{S}$$

Now we apply eq. 3.6 only for one sub-aperture, so we get a sub-focused image due to the fact that we are combining only some point of the synthetic aperture:

$$y(na, nr)_{sub} = \sum_{k=-l}^{+l} d(na+k, nr) \cdot h_s^*(nr, na+k, r) \quad l \in [-\frac{L_{s_{sub}}}{2}dx, \frac{L_{s_{sub}}}{2}dx] \quad (3.8)$$

for every point (na, nr) with bounds expressed in eq. 3.7. Each sub-summation takes into account only a portion of the synthetic aperture and gives a sub-image with azimuth resolution equal to

$$\rho_{az_{sub}} = \frac{L_a}{2S}$$

because we are using a synthetic aperture S time smaller than the nominal one. Now there is the problem to reconstruct the original back-projected signal, i.e. the final focused image expressed in eq. 3.6, from the expression of eq. 3.8. This can be done in a very simple way using the Fourier Transform. To understand this, suppose to have a generic time discrete signal $x(n)$ with N bins; its DTFT is

$$X(e^{j\omega}) = \sum_{n=-\frac{N}{2}}^{+\frac{N}{2}} x[n]e^{j\omega n}$$

It is clear that we can obtain the same result if we break the expression above in a sum of summation like

$$X(e^{j\omega}) = \sum_{k=0}^{S-1} \sum_{n=-\frac{N}{S2}}^{+\frac{N}{S2}} x[n + k\frac{N}{2S}]e^{j\omega n}$$

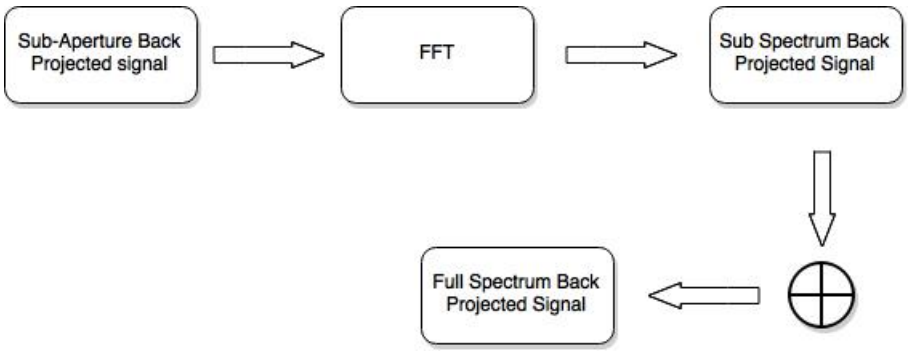

Figure 3.4: Logical flow to reconstruct the entirely back projected signal

If we apply the same concept to the sub-aperture problem, so if we sum coherently the DFT of each sub-aperture we obtain the DFT calculated over the whole synthetic aperture length. So the reconstruction formula is

$$y(na, nr) = \sum_{k=0}^{S-1} IFFT\Big(\sum_{na=-\frac{Ls}{S2}dx}^{+\frac{Ls}{S2}dx} Y_{sub}(ka + k\frac{L_S}{S}, kr)\Big) \tag{3.9}$$

Where $Y_{sub}(ka, kr)$ is the DFT of 3.8. In picture 3.5 there's a plot of a single range focalized spectrum and the spectrum obtained by summation of successive sub-aperture spectrums.

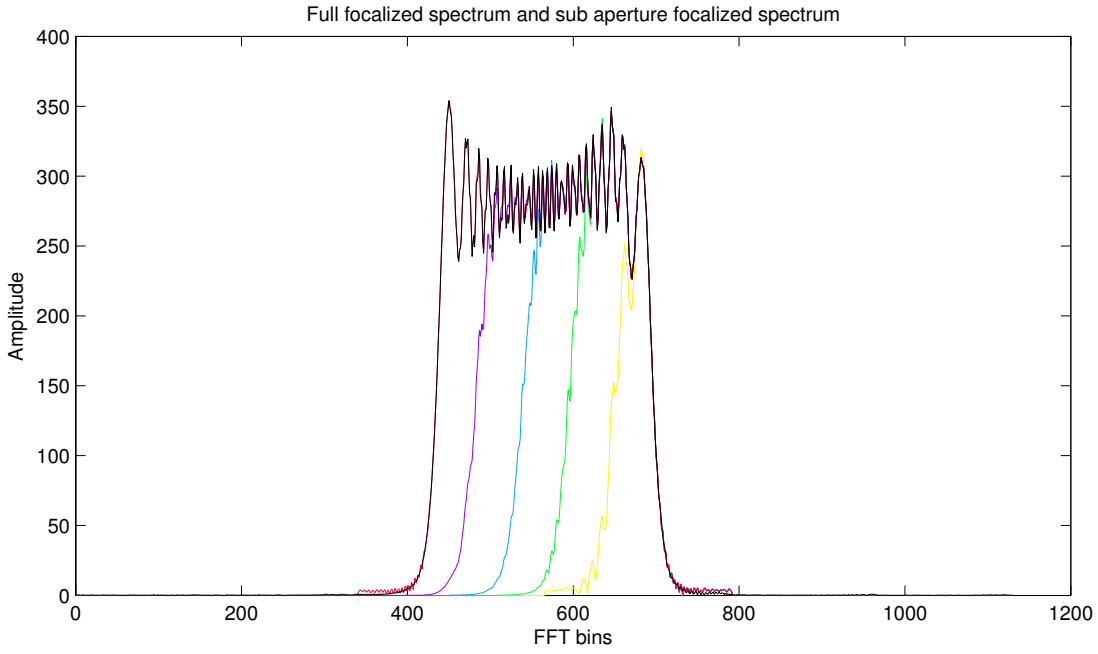

Figure 3.5: Effect of successive summation of sub apertures spectrum, the first is the yellow one and the last application is the red one that overlaps the black spectrum obtained using all synthethc aperture samples

The next figures illustrate how the sub-images of each sub-aperture appears in the case of a point-like target positioned in the middle of the image coordinates and $S = 5$ sub-apertures. To demostrate that the final image has the same resolution and gives the same results, we compare the main lobe of the focused image

using the two method and we plot the phase error of the reconstructed spectrum. Obviously the same system parameters are used to make the matching.

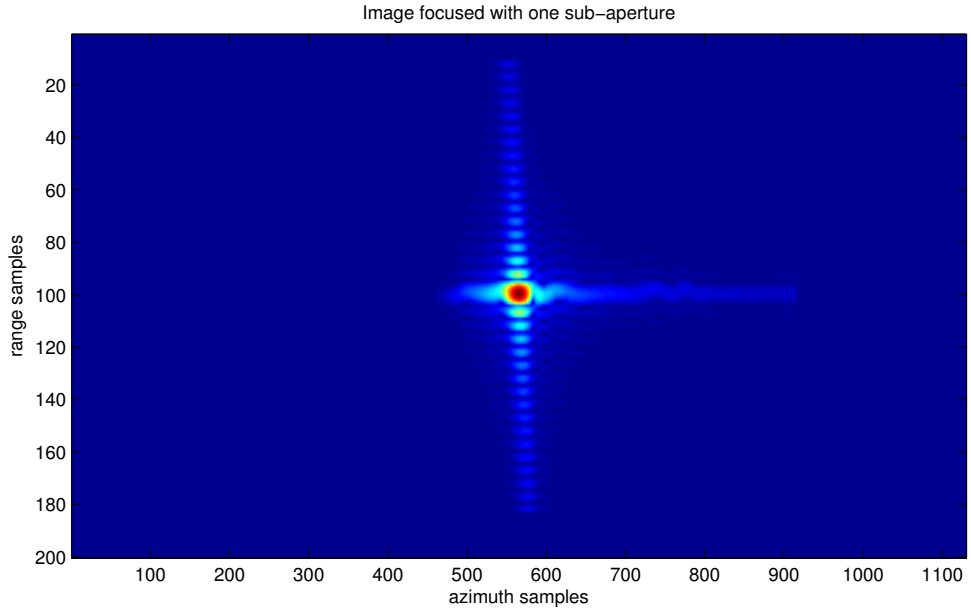

Figure 3.6: First sub-aperture focused sub-image.

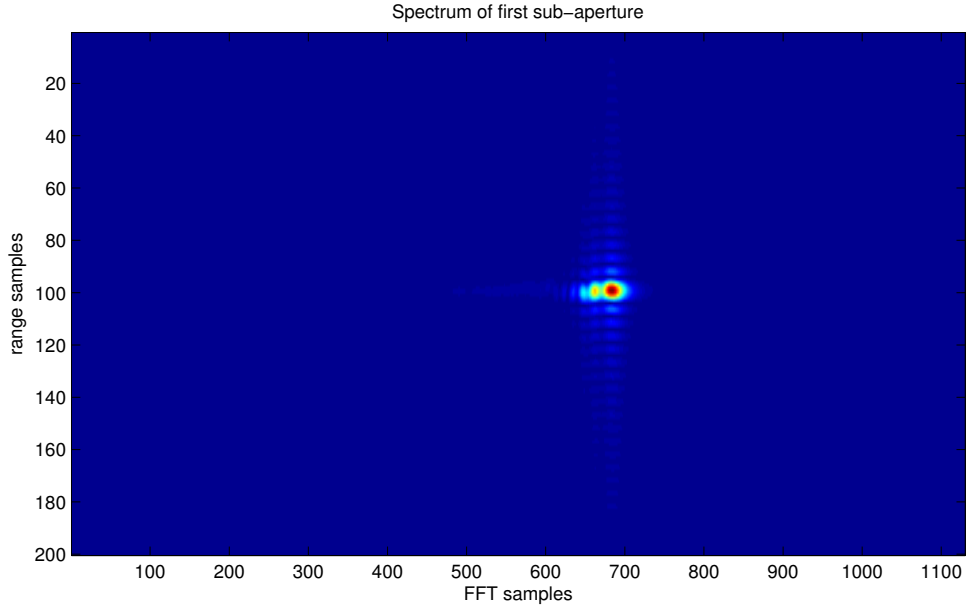

Figure 3.7: First sub-aperture focused sub-image spectrum.

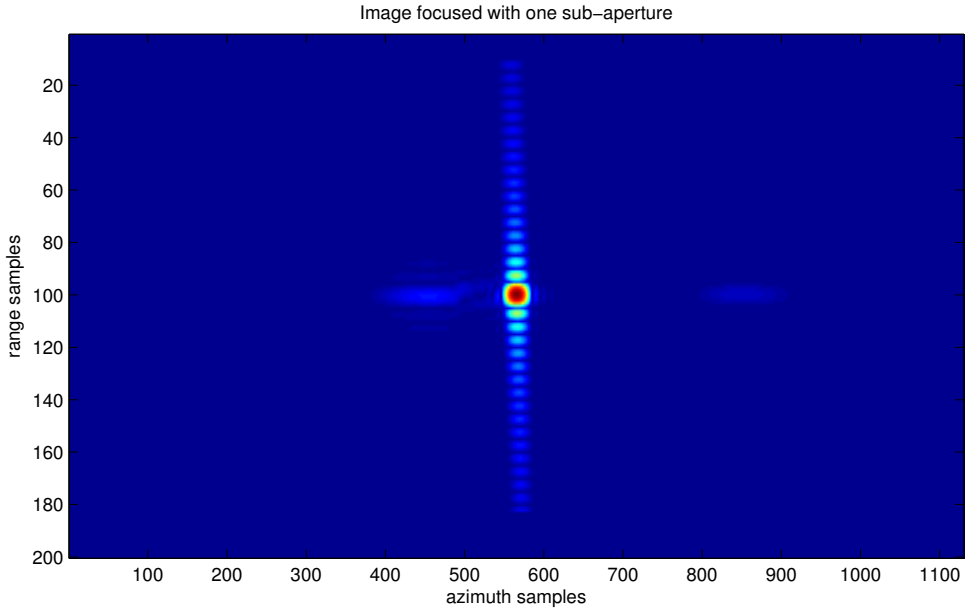

Figure 3.8: Second sub-aperture focused sub-image.

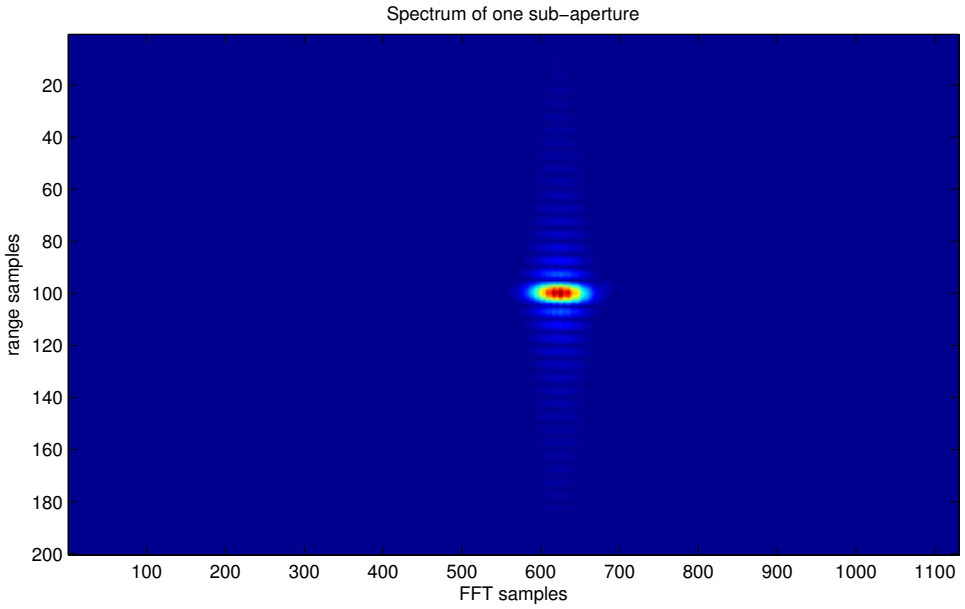

Figure 3.9: Second sub-aperture focused sub-image spectrum.

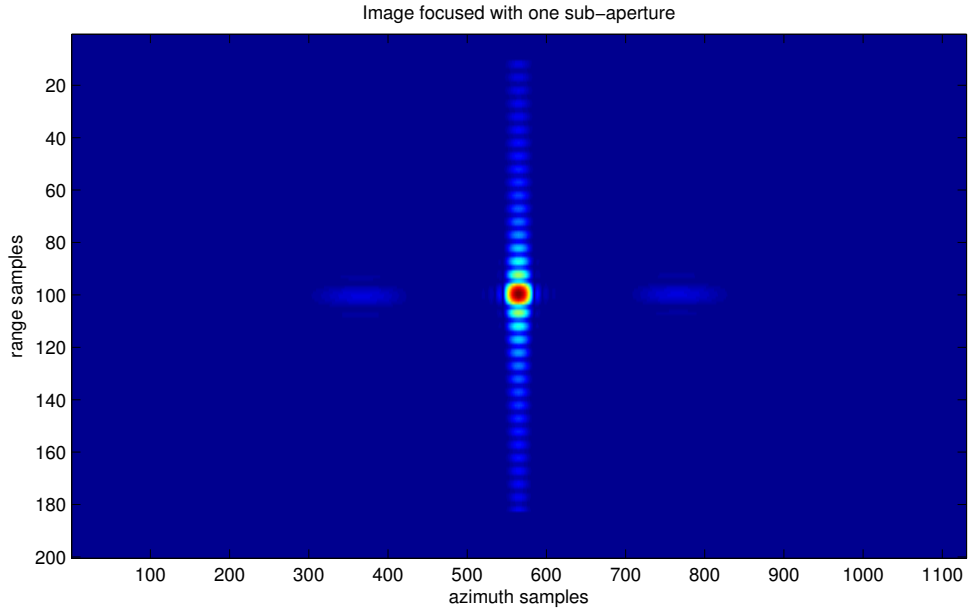

Figure 3.10: Third sub-aperture focused sub-image.

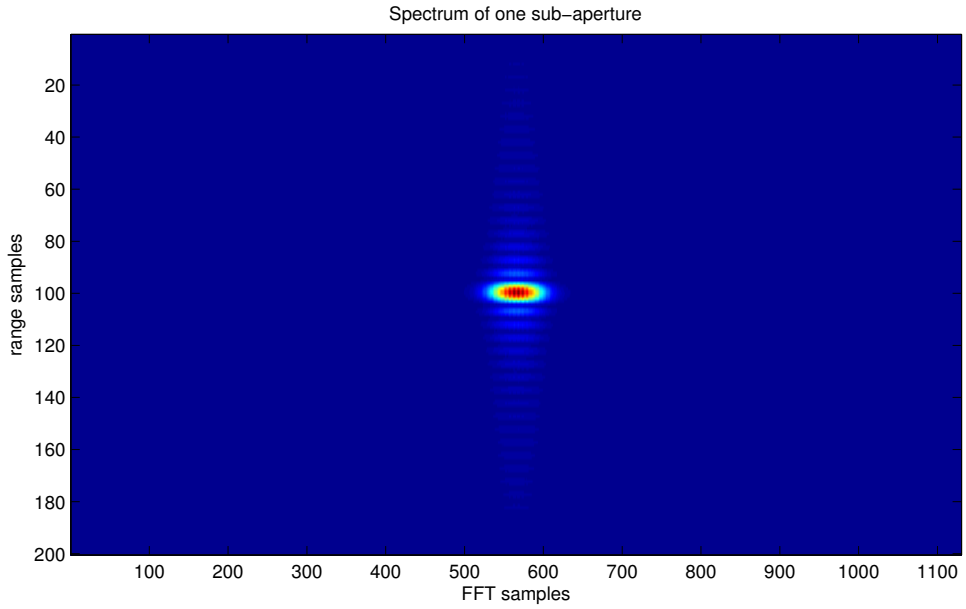

Figure 3.11: Third sub-aperture focused sub-image spectrum.

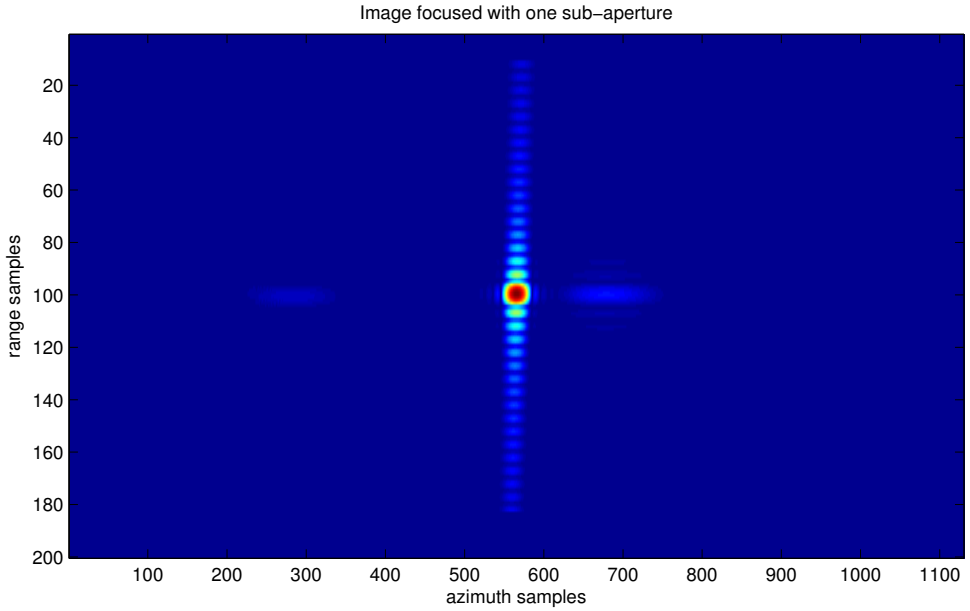

Figure 3.12: Fourth sub-aperture focused sub-image.

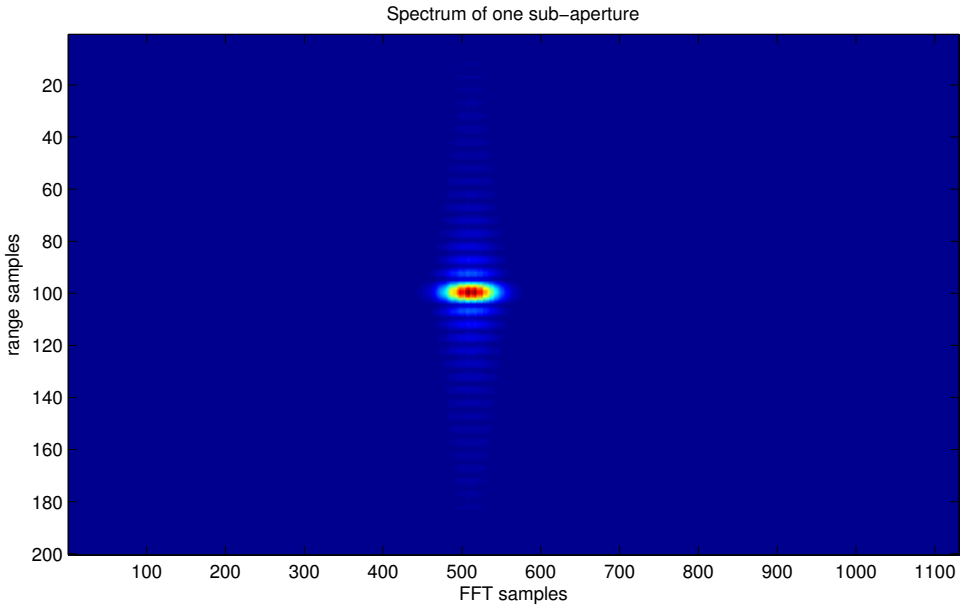

Figure 3.13: Fourth sub-aperture focused sub-image spectrum.

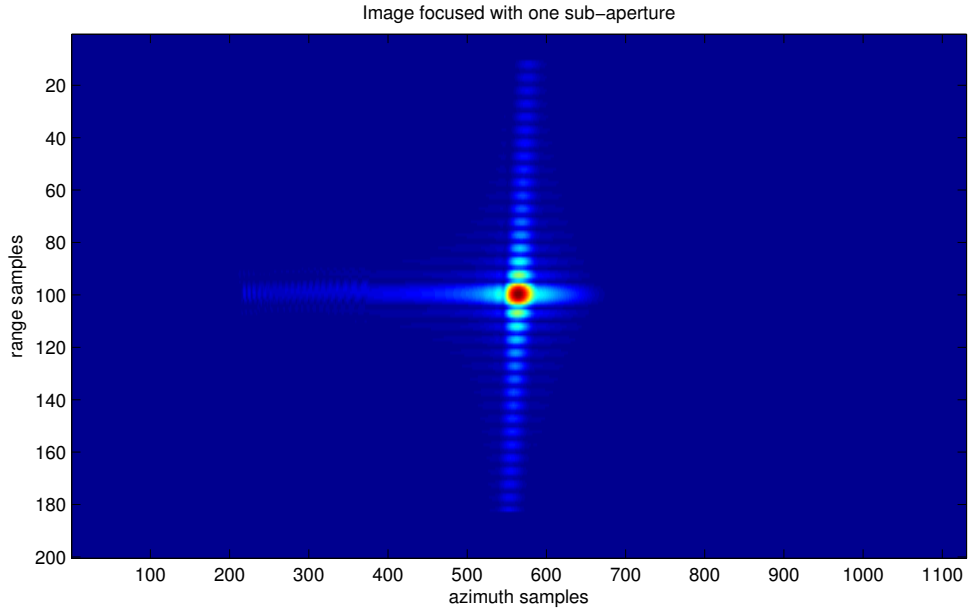

Figure 3.14: Fifth sub-aperture focused sub-image.

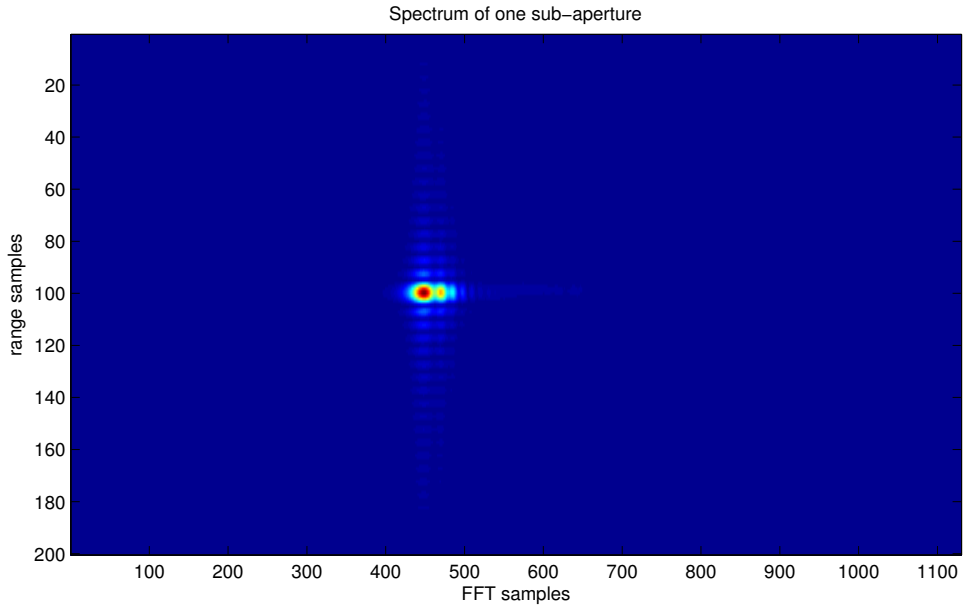

Figure 3.15: Fifth sub-aperture focused sub-image spectrum.

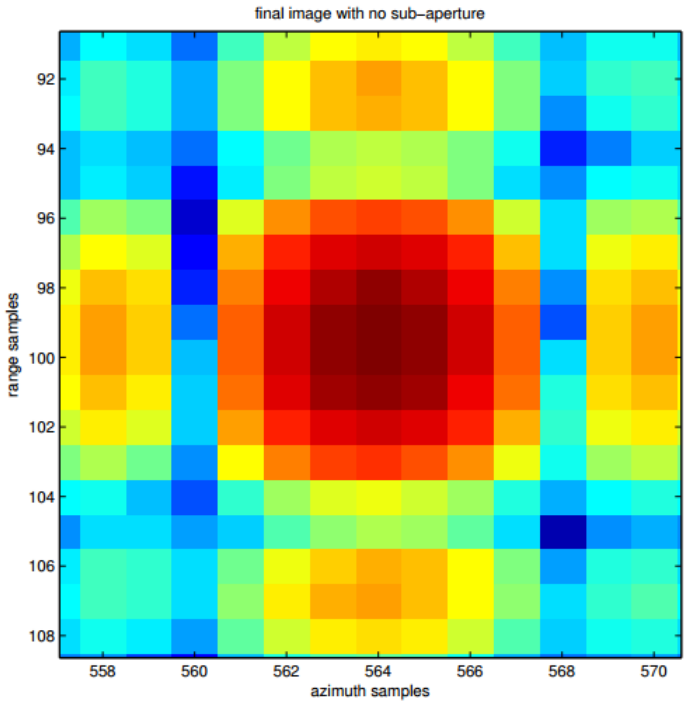

Figure 3.16: Main lobe of focused image using full back-projection method.

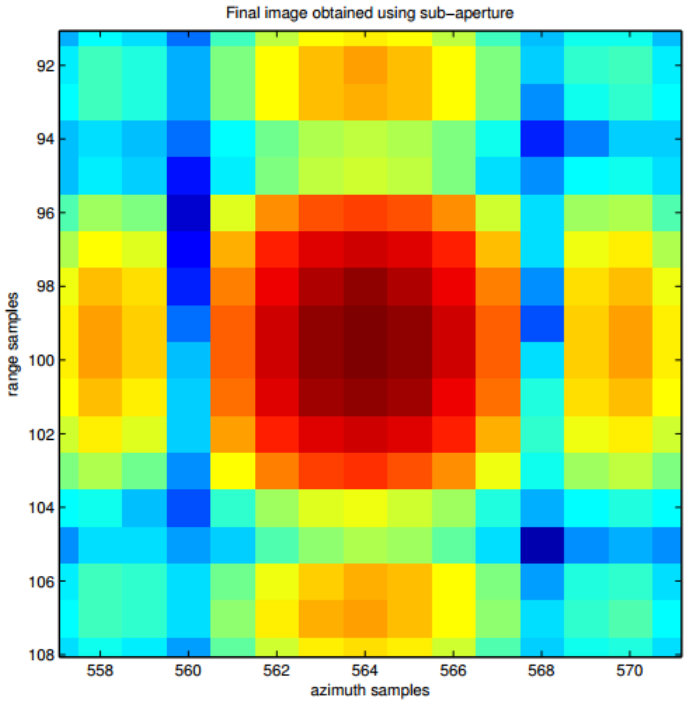

Figure 3.17: Main lobe of focused image using sub-aperture back-projection method. The two image are equal and so they have the same resolution.

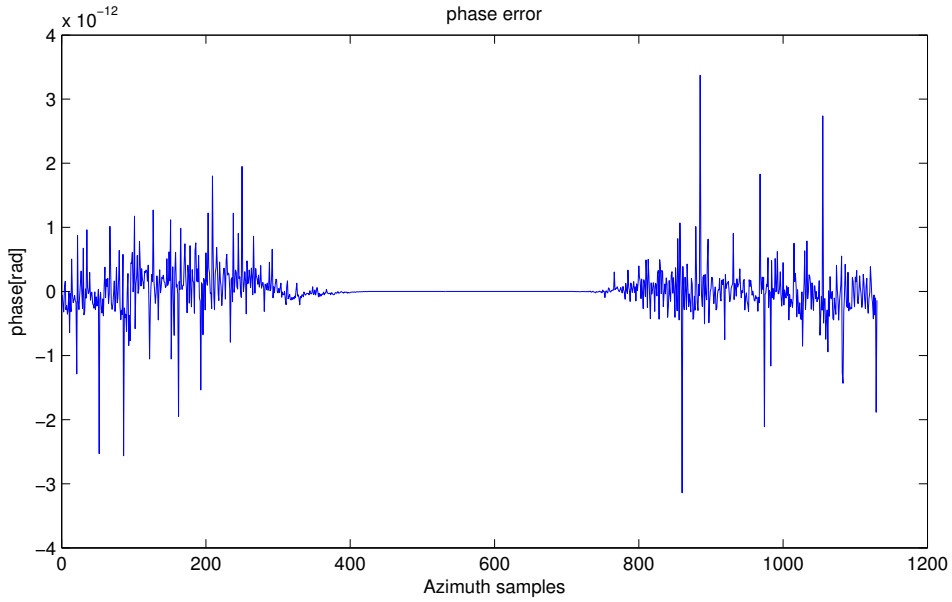

Figure 3.18: Phase error between the two spectrums. The values are in order of 10^{-12}, so we can say that the two spectrums are equivalent.

Chapter 4

Subsampling sub-aperture back projection focusing

The sub-aperture back-projection algorithm shown in chapter 3 doesn't give any profit in terms of calculation cost respect to the standard algorithm because we have only broken the summation in sub-summations but, in anyway, we make exactly the same number of operations. The idea is to add a sub-sampling stage to the previous algorithm in order to obtain a gain in computational cost.

4.1 Sub-aperture back-projection parameters

To obtain a computational performance gain we make a sub-sampling of the imaged azimuth point in the focusing stage. The idea is that if we divide the signal in S sub-apertures we can sub-sample each of them by a factor S and, in anyway, we are able to reconstruct the orignal full synthetic aperture spectrum and so the full resolution image. It is necessary to interpolate the data of each sub-aperture before reconstructing the spectrum and it is also necessary to place each sub-part of the spectrum in the correct position. In the following figure a scheme of the logical signal processing is shown.

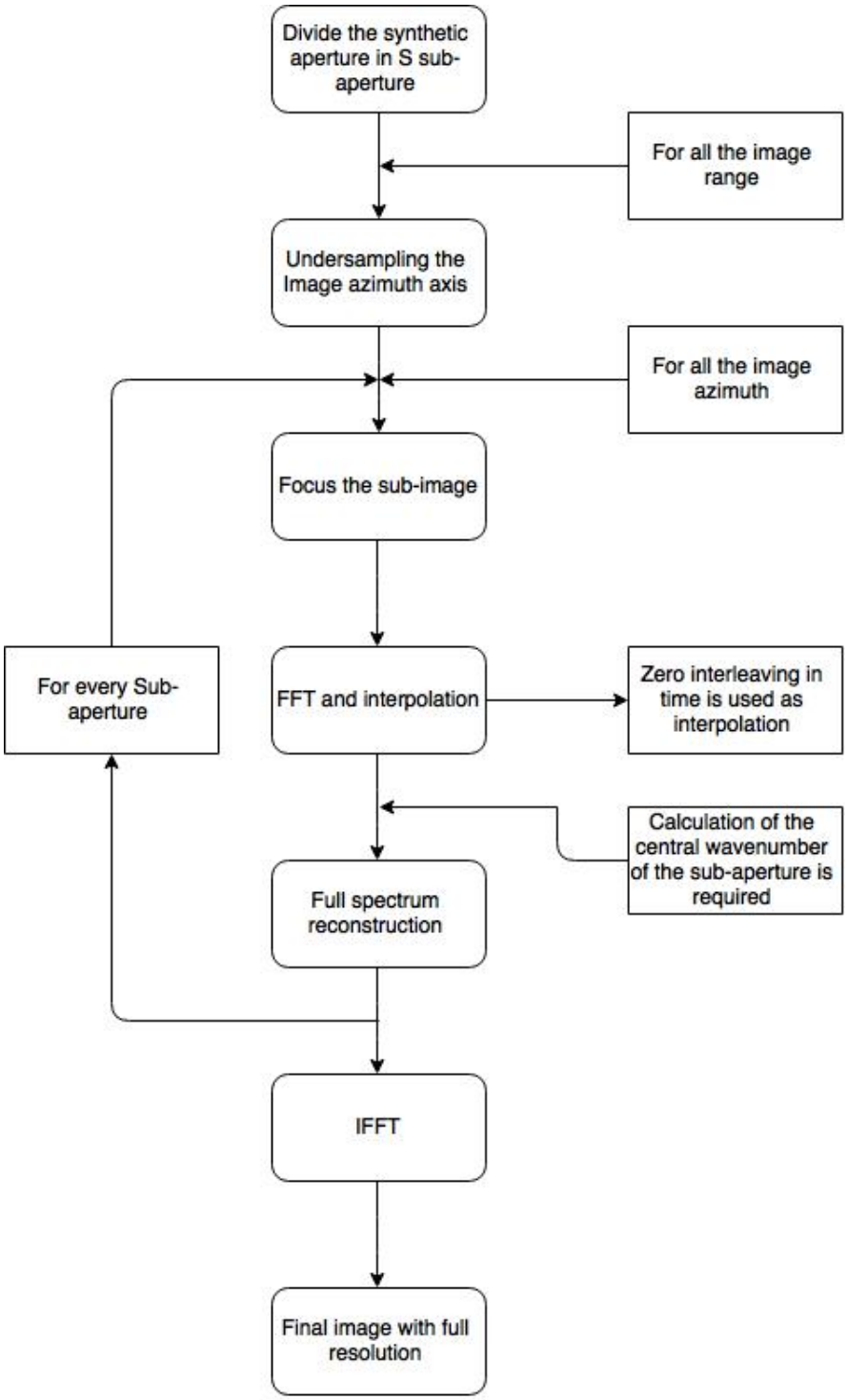

Figure 4.1: Logical scheme of the processing that is used in our focusing algorithm.

As pointed out from figure 4.1 the first step of the algorithm is to divide a synthetic aperture in S sub-apertures. The aperture length, like shown in equation 1.2, depends on the real azimuth size aperture, the wavelength λ and the range R_0. Now the range depends on the pixel that we want to focus and R_0 is the range refers to the middle range points in the final image. Saying that our image range extension is M pixels and saying

$$r = nr \cdot dr \quad with \quad nr \in [-M/2, M/2]$$

our synthetic aperture length is:

$$A = \frac{\lambda}{L_a} \cdot (R_o + r) \tag{4.1}$$

If we want to obtain S sub-apertures we have to divide 4.1 in S parts to get the *sub-aperture length.*

$$A_{sub} = A/S$$

It's very important that each sub-aperture doesn't contain the bins of the adjacent sub-apertures beacuse, in this case, we overlap these bins leading us to make an error in the focusing process. However the overlap between the sub-apertures isn't an error. In fact, if we make a windowed overlap, we can obtain some benefits. In the simulation we made an overlap equal to half the sub-aperture length so, in terms of antenna samples we have:

$$N_{overlap} = \frac{A_{sub}}{2dx}$$

In the next table there are the main parameters that are used to make the figures that follow.

Parameter	Symbol	Value
Wavelength	λ	0.25 $[m]$
Azimuth sampling	dx	0.5 $[m]$
Range sampling	dr	3 $[m]$
Antenna Length	L_a	4 $[m]$
Nominal distance to ground	R_0	3 $[km]$

Table 4.1: Table of system parameters

4.2 Sub-apertures Formation

The first step of the algorithm is the sub-apertures formation, i.e. the logical division of the whole synthetic aperture. After fixing S, we can calculate the already mentioned *sub-aperture length*:

$$A_{sub} = A/S$$

after that we find the bounds of each sub-aperture, called A_{inf_i} and A_{sup_i}. These values specify the length and position of each i-th sub synthetic antenna. These values are refered respect to the center of the synthetic antenna denoted as A_C; the scheme of such division is explain in the next figure 4.2.

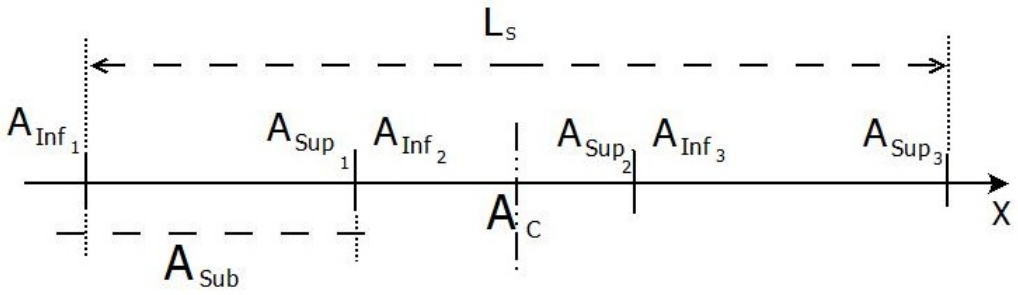

Figure 4.2: Logical scheme of the sub-aperture formation and division with $S = 3$. A_C is the middle point of the synthetic aperture of length L_S

The next step of the algorithm is to decide how much overlap we want between the sub-apertures. We refer to this quantity as $N_{overlap}$. This is an important feature beacuse a "clean cut" of the segments means to applies a square windows in x (azimuth) coordinate and this produces a lot of side lobes in the Fourier Transform domain. We decide to use a raised cosine window with

$$N_{overlap} = \frac{A_{sub}}{2}$$

in this way we get a more gentle segmentation, so we can reduce the effect of these side lobes. It is also very important that the windows summation is always unitary in order to prevent "interference" between the spectrum components of the sub-apertures:

$$\sum_{n=-\frac{N}{2}}^{\frac{N}{2}} RC(n - k * A_{sub}) = 1 \quad with \quad k = 1, 2, ...S \tag{4.2}$$

With overlap the bounds A_{inf_i} and A_{sup_i} are extended each for a quantity equal to $N_{overlap}$. We now refere to this quantities as $A_{S_{bot_i}}$ *and* $A_{S_{top_i}}$. Note that the sub-apertures at the edges of the array have only one direction, toward A_C, on which they can expand. An example of such windows in azimuth dimension are shown in figures 4.3 and 4.4

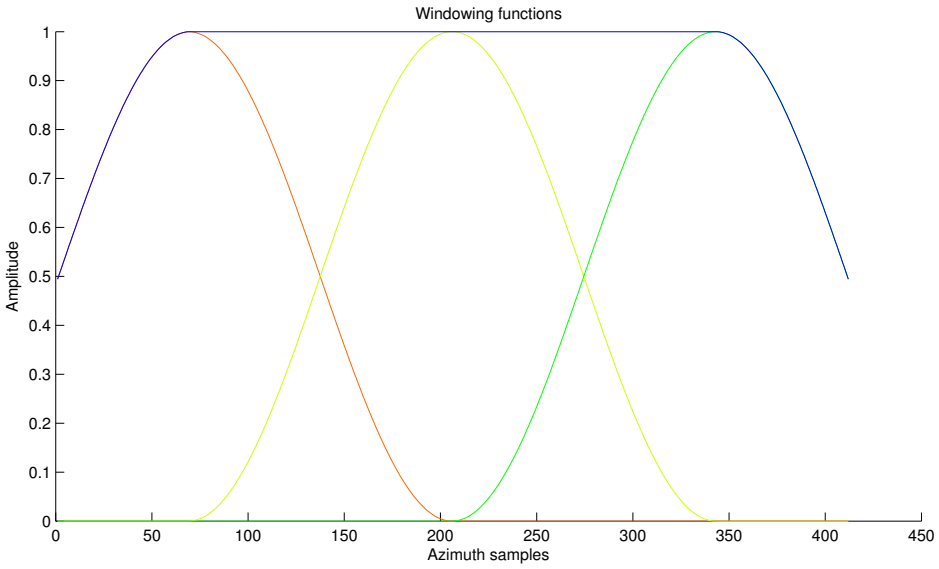

Figure 4.3: Window functions with $S = 3$, in blue the sum of the windows is plotted.

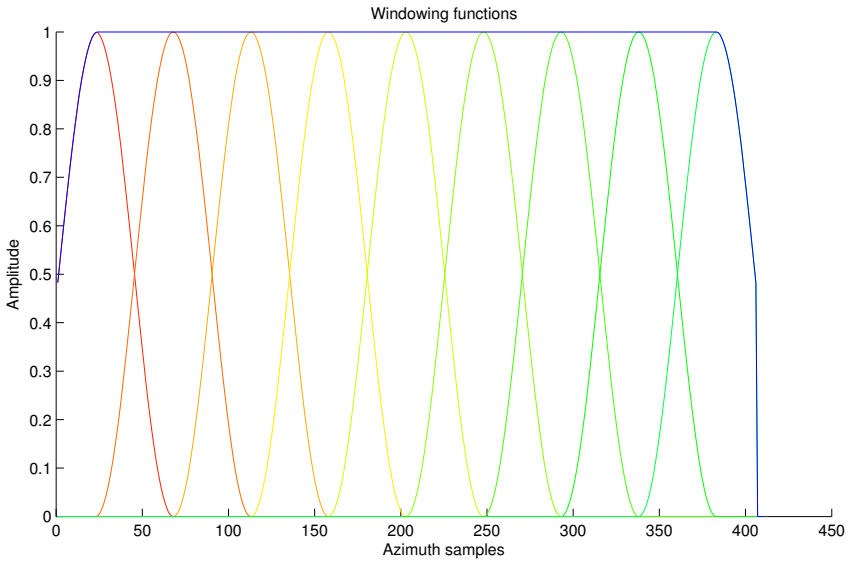

Figure 4.4: Window functions with $S = 9$, in blue the sum of the windows is plotted.

4.3 Subsampling sub-aperture back projection

Now we have all the elements to talk about the sub-sampling process of the image azimuth points. This stage is the one that allows to obtain the speed up in the back-projection algorithm. What we do is simply to apply the equation 3.8 but now, instead of back-projected every point in the image like in eq. 3.7, we focus one point every S. This means that now the sampling interval dx is S time larger than before. We can rescribe equation 3.8 as:

$$\begin{cases} y(na, nr)_{sub} = \sum_{k=-l}^{+l} d(na+k, nr) \cdot h_s^*(nr, na+k, r) \quad for \quad na = S \cdot i \\ \qquad\qquad with \quad i = -N/2, -N/2+1, ..., -1, 0, 1, ..., N/2-1, N/2+1 \\ 0 \qquad elsewhere \end{cases} \tag{4.3}$$

in which:

$$l \in [A_{S_{bot_i}}, A_{S_{top_i}}]$$

specifies the antenna samples used in the single sub-aperture focalization. The focused data are stored in a matrix with dimensions MxN, so we can think to initialize this matrix with all zeros and than focused a point every S. In this way we obtain an undersampled version of 3.8 with S zeros between two samples. This means that we have done a *zero interleaving* operation that is necessary to

restore the sampling frequency at the nominal $1/dx$ value after the sub-sampling stage. An example can be seen in the next figure, in which there is a focused image for a fixed range and a single sub-aperture.

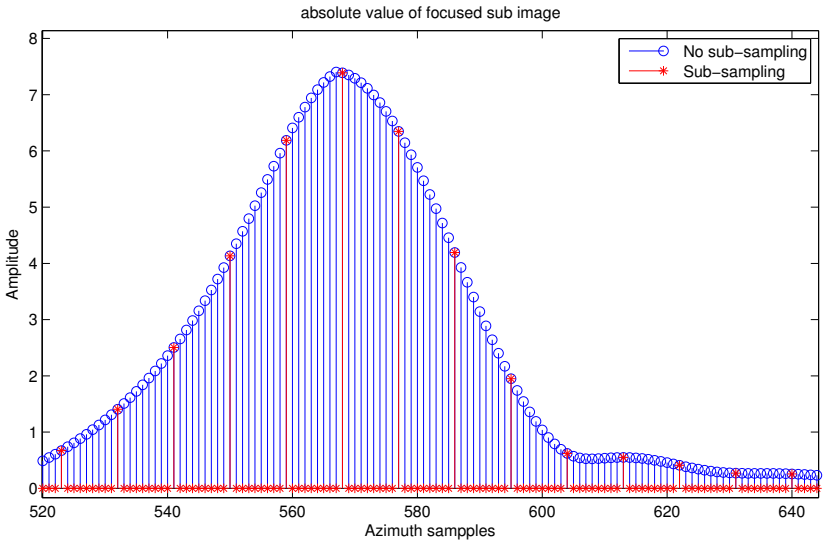

Figure 4.5: Zoomed focused image for a single sub-aperture with $S = 9$, both with and without sub-sampling.

In equation 3.9 we sum the spectral components of each sub-aperture to reconstruct the full spectrum. Now we have an under-sampled signal with zero-interleaving so, when we make the DFT of such signal, we get a periodic spectrum in the frequency domain with period $\frac{2\pi}{dx \cdot S}$ [4]. To reconstruct the full spectrum we take a single replica of the periodic spectrum and we put it in the right spectral position. Each replica is shifted respect to the central wavenumber $\frac{2\pi}{dx \cdot S}$ by a quantity that can be derminated by eq. 2.5. In fact in the focusing operation expressed in eq. 4.3 we have corrected all the phase terms due to the sensor motion respect to the target and so, if $R_0 \gg (x - x_p)$ then eq. 2.5 holds also for the focused data. Fixed a certain sub-aperture, like expressed in figure 4.6, knowing the distance between the image point we want to focus and the synthetic aperture and knowing the distance between the image point azimuth position A_C and the central azimuth position of i-th sub-aperture $A_{SUB_{C_i}}$ we get:

$$K_{xi} = \frac{d\phi(x)}{dx} = \frac{4\pi}{\lambda} \frac{(A_C - A_{SUB_{C_i}})}{R} \qquad [rads/m] \tag{4.4}$$

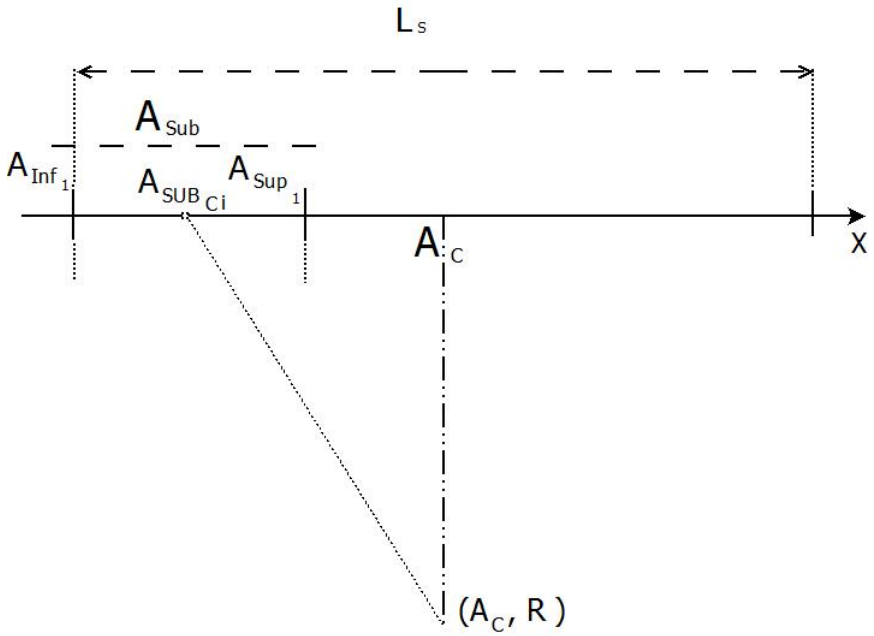

Figure 4.6: 2D geometry of the central wavenumber for a given sub-aperture. R is the distance from the target and A_C is the target azimuth coordinate equal to the synthetic aperture central point.

Note that if the azimuth pixel position that we want to focus is equal to A_C, i.e. we center the synthetic aperture on that pixel, the azimuth distance between the sub-aperture center and the synthetic aperture center is exactly $A_{SUB_{C_i}}$. From equation 4.4 we can calculate the frequency shift of each sub-aperture respect to the zero frequency component that occurs at the mid point in the synthetic aperture. We suppose now that the zero frequency component is placed at the middle position of the spectrum matrix, that is $N/2$. So from equation 4.4 the frequency component at position A_C is equal to zero and it is stored in spectrum matrix at position $N/2$. The steps to obtain the full back-projected spectrum are explained in the following.

Replica selection The DFT of a single sub-aperture, after the zero interleaving interpolation, has a periodic spectrum so the first step is to take a single replica of $Y_{sub}(ka, kr)$ that is the DFT of eq. 4.3. To do this we calculate the central wavenumber relative to the center of the sub-aperture with formula 4.4. We convert this wavenumber into frequency samples by:

$$N_{kx_i} = \frac{K_{xi}}{\frac{2\pi}{dxN}} \tag{4.5}$$

where $\frac{2\pi}{dxN}$ is the sampling period in wavenumber and N is the number of azimuth samples and it is also the number of the sub-aperture DFT samples. If the whole sub-spectrum has N samples and a sub-aperture is taken

dividing a synthetic aperture in S parts, so a single spectral replica has N/S samples. So the spectrum of a single sub-aperture replica is obtained taking N/S samples of its DFT centered on $N/2 + N_{kx_i}$, where, as said before, $N/2$ is the discrete index relative to the zero frequency component.

$$\begin{cases} Y_{sub_w}(ka, kr) = Y_{sub}(ka, kr) \quad for \quad ka \in [N/2 + \frac{N_{kx_i}}{2} - N/S, N/2 + \frac{N_{kx_i}}{2} + N/S] \\ 0 \qquad elsewhere \end{cases} \tag{4.6}$$

This operation is like to applying a square window of N/S samples centered on $N/2+N_{kx_i}$ on the periodic sub-aperture spectrum. The next figure shows an example of $Y_{sub}(ka, kr)$ with fixed kr and shows the replica selection.

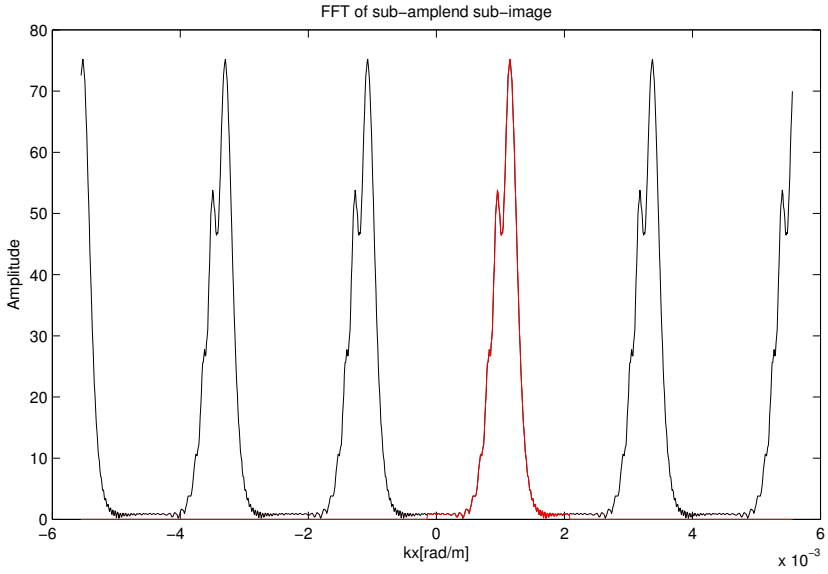

Figure 4.7: Example of focused DFT with sub-sampling factor $S = 5$. In black the whole FFT is plotted, in red the selected replica relative to the first sub-aperture.

Full spectrum reconstruction The second step constist of taking the selected replica and putting it in the full spectrum matrix at the rigth spectral postion. To get the full reconstructed spectrum we sum the actual reconstructed spectrum with the selected replica placed in the position $N/2+N_{kx_i}$ that correspond to the central wavenumber of the i-th sub-aperture.

$$Y_{full}(ka + k, kr) = Y_{full}(ka + k, kr) + Y_{sub_w}(ka + k, kr) \tag{4.7}$$

We have to do this operation for the matrix points $k \in [N/2 + N_{kx_i}/2 - N/S, N/2 + N_{kx_i}/2 + N/S]$, $kr \in [-M/2, M/2]$ and for all the S sub-apertures.

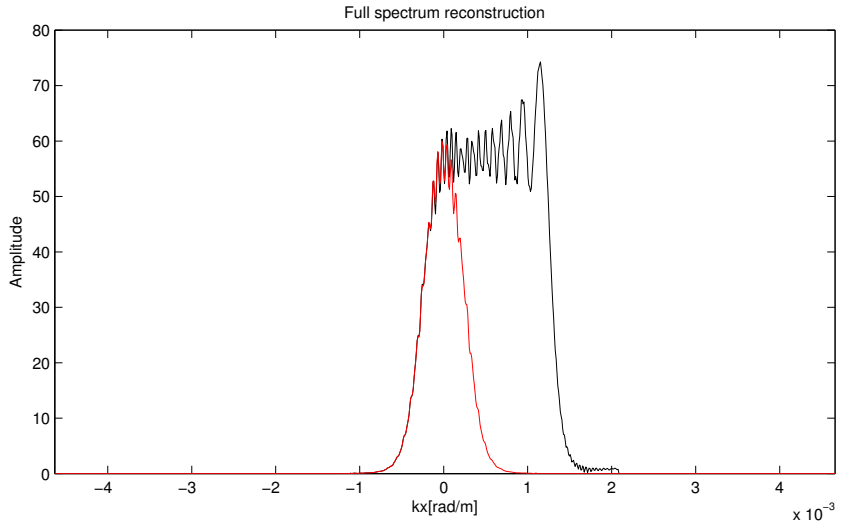

Figure 4.8: Example of full spectrum reconstruction for $S = 5$. In black the whole FFT is plotted in red the selected replica, that, in this case, is the one with $N_{kx_i} = 0$

So the final image is obtained by applying the IFFT to 4.7 after adding all the sub-aperture contributes. An example of focused image in the amplitude-azimuth domain is plotted in the following figure.

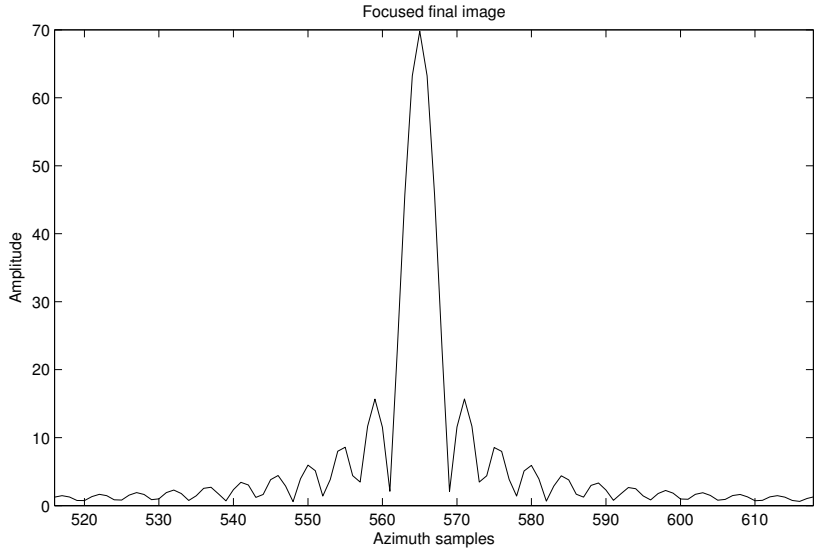

Figure 4.9: Zoom of focused final image with fixed range and $S = 5$.

The next figures show the final image obtained applying this algorithm with $S = 5$ and the image obtained using the "classical" back-projection.A sine-like trajectory

is used in both the two cases. The last figures shows the comparison between the main lobe of the final images and the phase error between the spectrum obtained in the two cases.

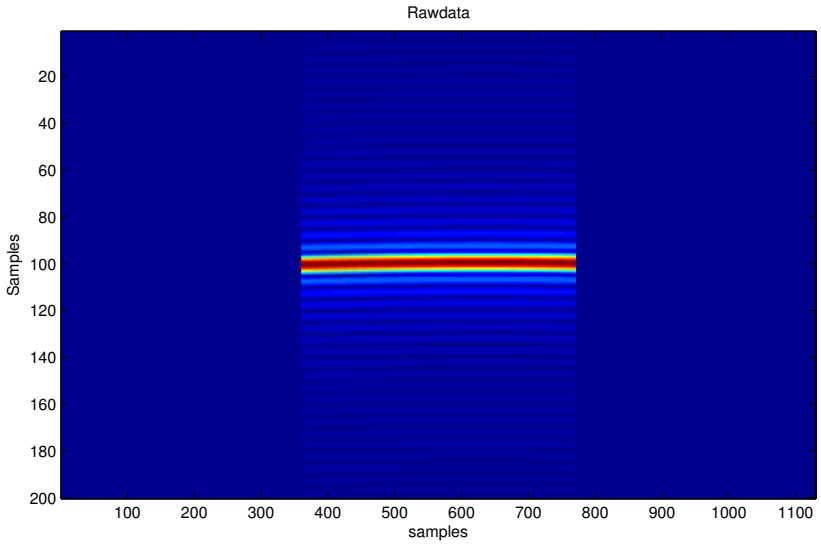

Figure 4.10: Rawdata.

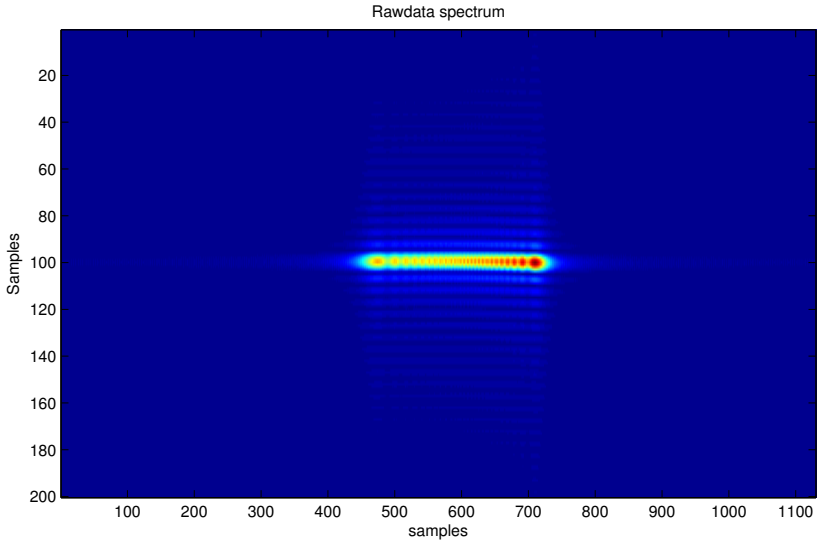

Figure 4.11: Rawdata spectrum.

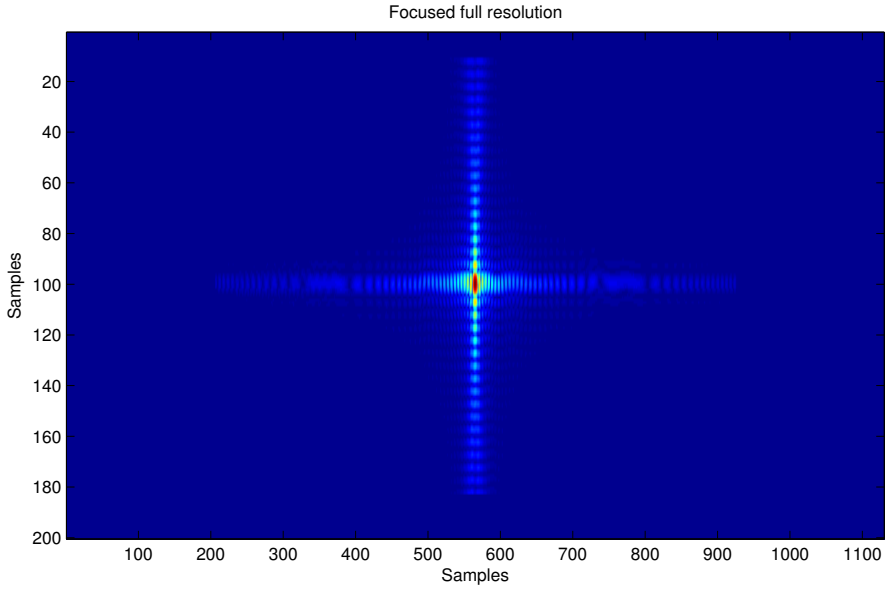

Figure 4.12: Focused image with full back-projection integral

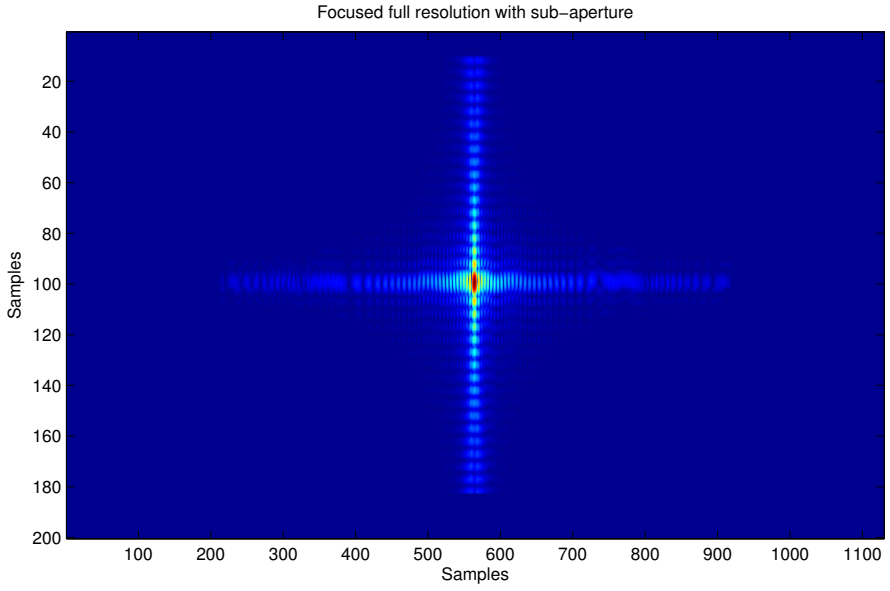

Figure 4.13: Focused image with sub-sampled back-projection integral

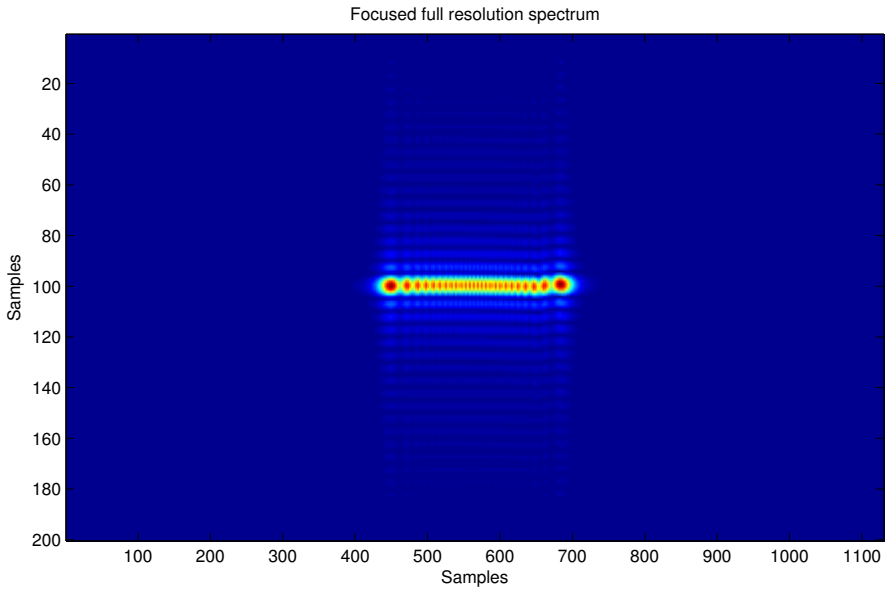

Figure 4.14: Focused image spectrum with full back-projection integral

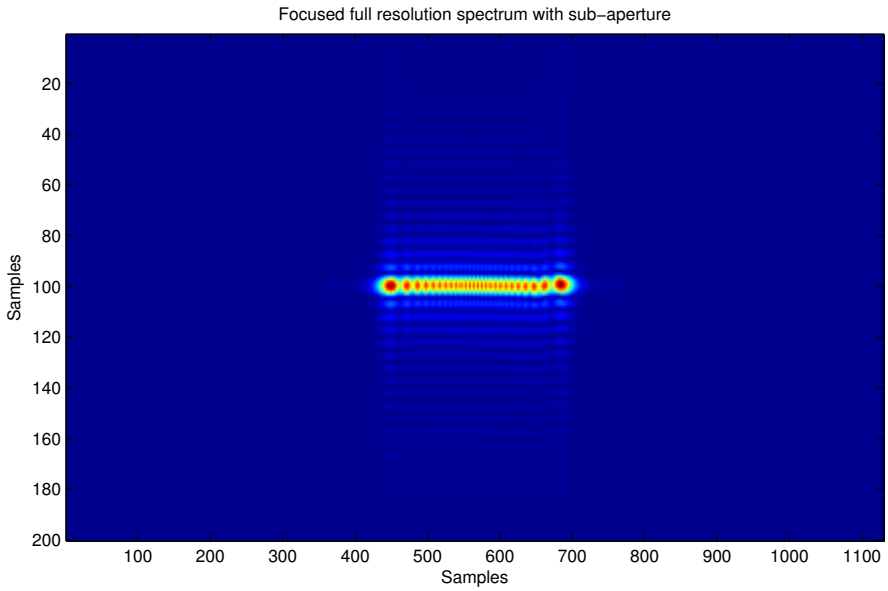

Figure 4.15: Focused image spectrum with sub-sampled back-projection integral

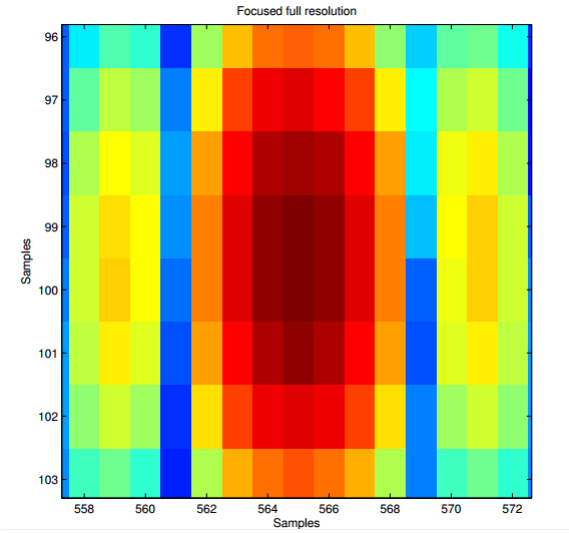

Figure 4.16: Zoom of the main lobe focused image obtained with the full back-projection

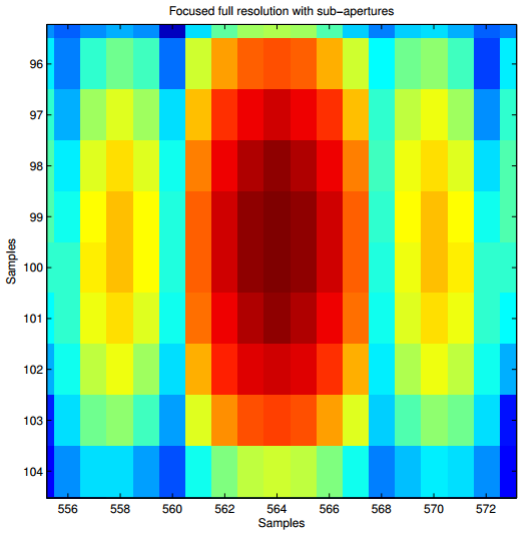

Figure 4.17: Zoom of the main lobe focused image obtained with the sub-aperture back-projection

To compare the performance of our algorithm respect to the full back-projection one we calculate the phase error between the two spectrums. For a fixed range we get this phase error

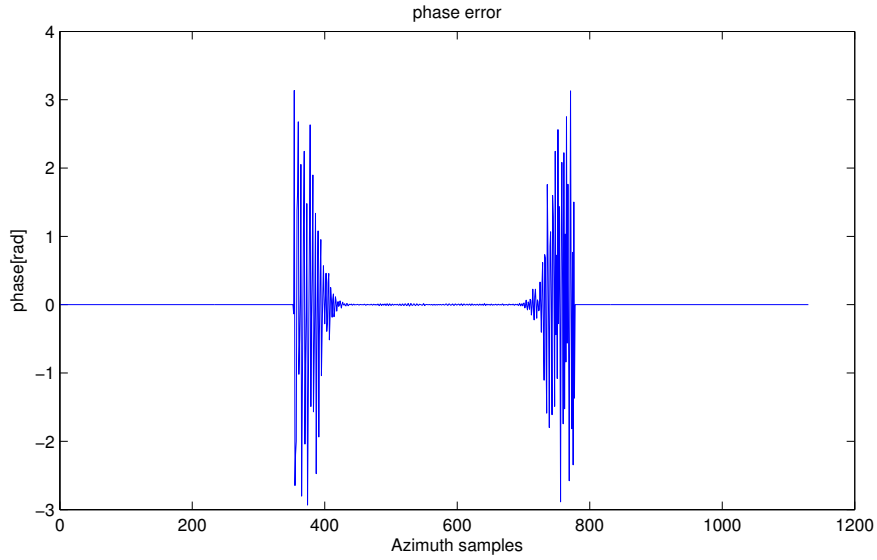

Figure 4.18: Plot of the phase error for a fixed range.

From figure 4.18 can be seen that we have, at some point, a phase error that vary from π and $-\pi$. This is because when we reconstruct the full spectrum with the sub-apertures we take a portion of the spectrum according to 4.5 and we sum it with other portions as in equation 4.7. A single spetral part is taken with a window operation and, in particular, a square window of length N/S centered on the right replica is applied. So the spectrum reconstruction is made by summation of finite length portions of sub-spectrums. At the edge of the spectrum, at a certain point, we have a reconstructed spectrum truncation due to the finite length of the windows. This truncation causes an imperfect summation of the side lobes and so it is like to have some ”noise” in the full reconstructed spectrum. The effect of this ”noise” is the phase error in the truncation position, like shown in figure 4.18.

Chapter 5

Performance analysis

After we talking about the subsampled back-projection algorithm and how it works to obtain the final image a natural question rises, that is: how much subsampling we can do? So we want to study the subsampling bound that ensures a low phase error in the final image spectrum and also ensures low side lobes in the final image.

5.1 Time-bandwidth product

In chapter 2 we talk about the frequency trend of the received signal. We derive the phase term modulation for a linear trajectory in eq. 2.5, and if we compute the derivative respect to the azimuth dimension we obtain a slope equal to

$$\frac{4\pi}{\lambda \cdot R_0}$$

This relation tells us that the frequency components have a constant slope so we get in frequency an azitmuh chirp. We can calculate the *space-bandwidth product* of that chirp in order to obtain some informations about the maximum subsampling factor we can use without gettin a phase error near the target position. In chapter 1 we said, from the linear array theory, that the maximum observable spatial frequency is:

$$f_{xM} = 2\frac{\sin \psi_M}{\lambda}$$

and the angular aperture is :

$$\Delta\psi = 2\psi_M = \frac{\lambda}{L_a}$$

The bandwidth is double to the maximum view angle due to the symmtrety of the problem, so the nominal bandwith, expressed in wavenumber, of the real antenna is:

$$B_{L_a} = \frac{2 \cdot \pi}{\lambda} \tag{5.1}$$

The space duration of that chirp is equal to the synthetic aperture L_S, in fact the received echoes out of this value are not correlated to the target that we are observing. So we refer to this space duration as

$$D = \frac{\lambda}{L_a} R_0 \tag{5.2}$$

With this two elements we can derive the space-bandwidth product BT for an ideal linear trajectory [4], and it is equal to the number of samples in azimuth of that chirp. If we want to calculate the time-bandwidth product we have to convert the chirp space duration to chirp time duration knowing the platform velocity v_s.

$$BT = D \cdot B_{L_a} = \frac{\lambda R_0}{L_a^2} \tag{5.3}$$

We consider now the sub-apertures case, sure that the eq. above has to be modified to account the less duration of each sub-aperture. Now fixing the S parameter we suppose that the sub-apertures are each of lenght

$$A_{sub} = A/S$$

so a squared window is applied in space. In a first approximation the duration of each sub-aperture is

$$D_{sub} = \frac{D}{S}$$

and the bandwidth is

$$B_{L_{a_{sub}}} = \frac{B_{L_a}}{S}$$

If we invert this relation we get the sampling interval

$$dx_s = \frac{S}{B_{L_a}}$$

and the number of samples of each sub-band becames

$$N_{BT_{samples_{sub}}} = \frac{D_{sub}}{dx_s} = \frac{BT}{S^2} \tag{5.4}$$

This equation shows that in the ideal case the number of samples required of each sub-band has a reduction factor of S^2, that is the one we expected to obtain. Consider now that each sub-band is taken applying a square window function like

$$f(x) = rect(\frac{x}{D_{sub}})$$

it is well known that its fourier transform is a *sinc* function as

$$F(f) = sinc(D_{sub} f)$$

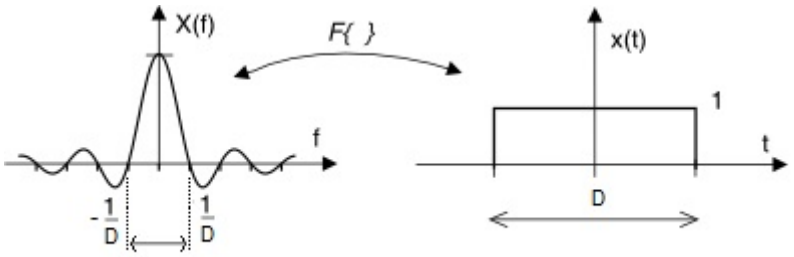

Figure 5.1: Square window and its fourier transform, the bandwidth of the main lobe is $1/2D$

A window operation in time becames a convolution operation in frequency, and this cause an expansion of the bandwidth and so it cause a decrease in the sampling period. In a first approximation we consider only the bandwidth of the main lobe equal to $\frac{2S}{D}$. The rectangular bandwidth $\frac{B_{L_a}}{S}$ in frequency is now expanded by that quantity and becames

$$B_{L_{a_{sub}}} = \frac{B_{L_a}}{S} + \frac{2S}{D}$$

so the sampling period is now

$$dx_s = \frac{1}{\frac{B_{L_a}}{S} + \frac{2S}{D}}$$

and the number of samples for each sub-band, i.e. the space bandwidth product, is

$$N_{BT_{samples_{sub}}} = D_{sub} \cdot B_{L_{a_{sub}}} = \frac{BT}{S^2} + 2 \tag{5.5}$$

In chapter 1 we talked about the space sampling period in the azimuth direction dx. The number of samples taken onboard for each aperture can be expressed as the synthetic aperture length of eq. 1.2 over a factor dx:

$$A = \frac{L_S}{dx}$$

The number of samples processed for each sub-aperture is just

$$A_{sub} = \frac{A}{S^2}.$$

If we put this expression in 5.5 we obtain an estimation of the S parameter as

$$S_{max} = \sqrt{\frac{A - BT}{2}} \tag{5.6}$$

Equation 5.6 take into accounts only the first lobe of the *sinc* function and it is only valid for a linear trajectory. During the focusing process the phase term due to the fligth motion is corrects ans so we axpect that te equation 5.6 still holds on.

5.2 Simulation results

We want to extend now the speech of the previous section and compare it with the Matlab simulation. We start now to consider that in time we use a rised cosine window instead of a square one, so we have to analyze this effect. We use an overlap equal to half of the sub-aperture length as $N_{overlap} = \frac{A_{sub}}{2}$, this means that we have a rised cosine window with parameter $\beta \simeq 1$. Its fourier transform is so approximated as a *sinc* function and we can take into account only two secondary lobes as expressed in eq. 5.6 [3]. So we can think to use eq. 5.6 as bound of S in our simulation.

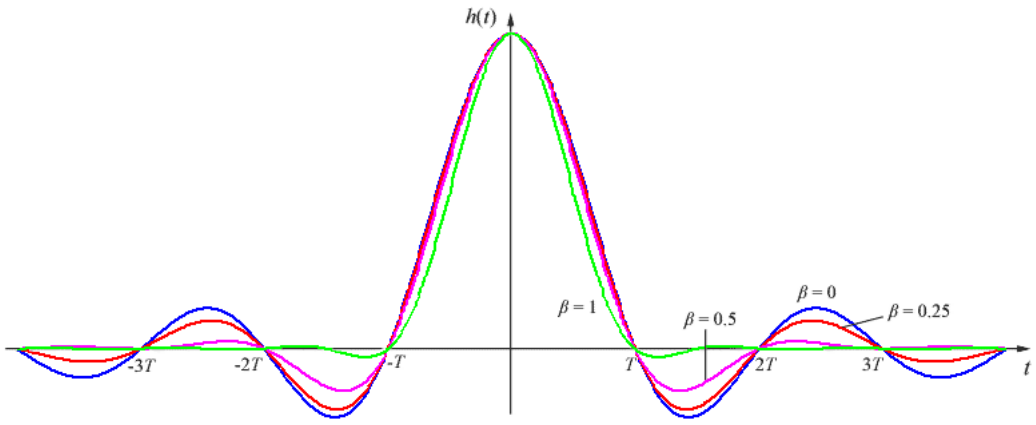

Figure 5.2: Fourier transform of a raised cosine window for some values of β parameter

In chapter 4 the table 4.1 explains the main parameters used in the simulations to get the images. With these parameters we obtain an S_{max} value equal to: 12.8087. We fix $S = 11$ and we add a sine like fligth trajetoctory as

$$\sin(2 * pi * (1 : N)/N)$$

the rawdata and its spectrum are the same as figures 4.10 and 4.11. Now we apply the focusing algorithm and we get the following images.

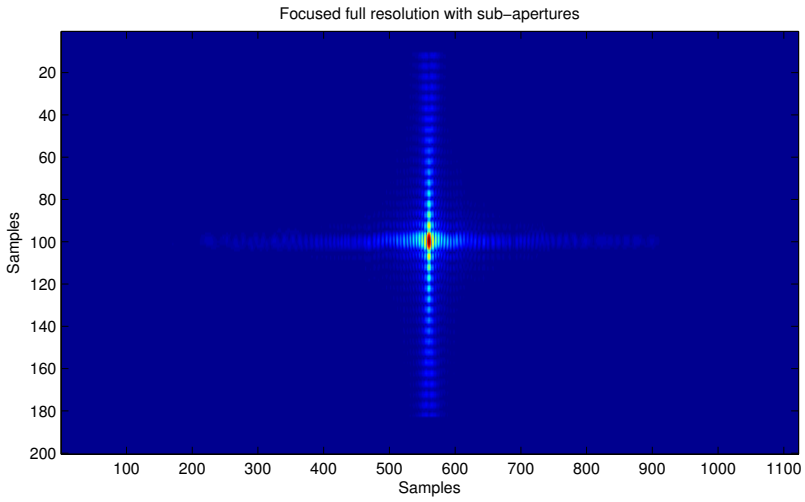

Figure 5.3: Final focused image with $S = 11$, the systems parameters are those of table 4.1.

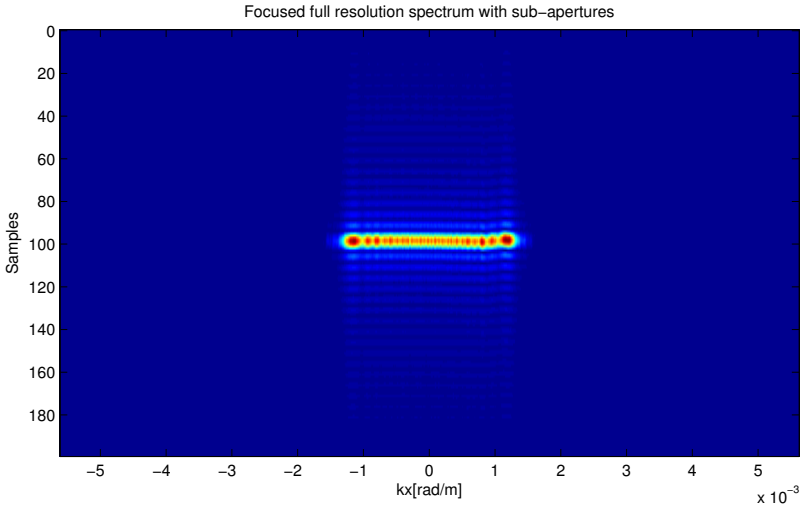

Figure 5.4: Final focused image spectrum with $S = 11$, the systems parameters are those of table 4.1.

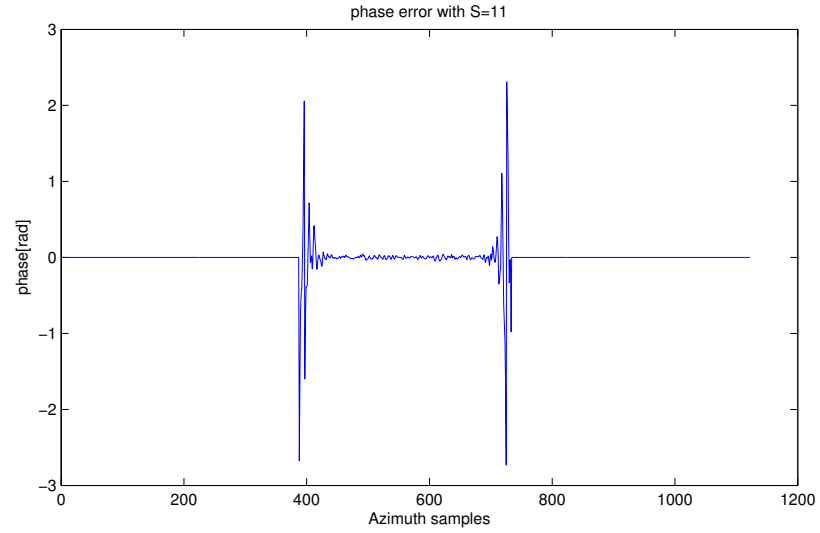

Figure 5.5: Phase error of the spectrum with $S = 11$ and the systems parameters are those of table 4.1.

The results show that in this case the phase error is very low near the target position. Now if we try to use a value of S above S_{max}, we obtain some errors in the final image. The following figures show the results of the algorithm obtained using $S = 15$.

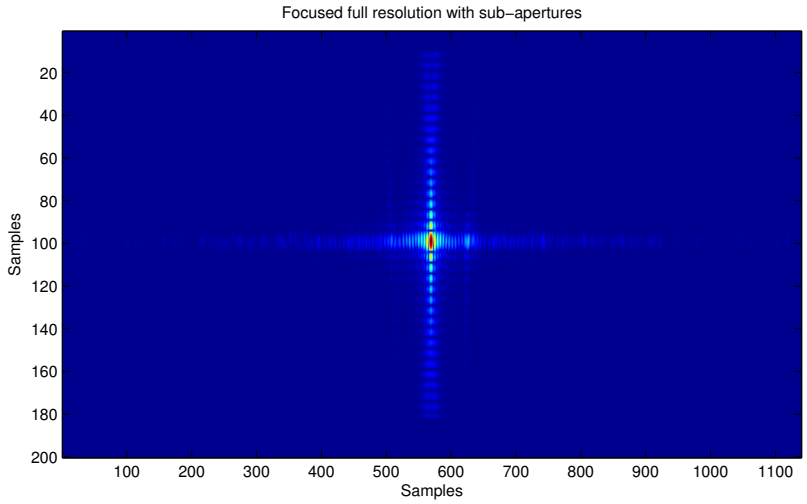

Figure 5.6: Final focused image with $S = 15$, the systems parameters are those of table 4.1. It can be seen that there are some errors and so S is too big.

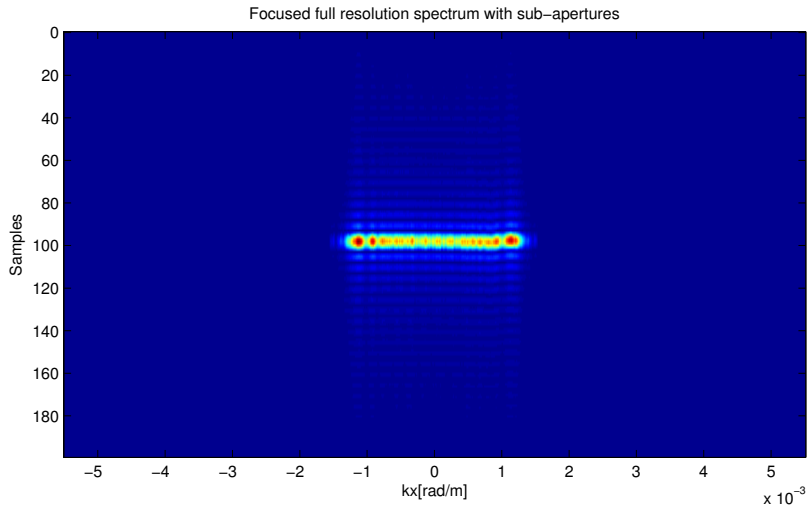

Figure 5.7: Final focused image spectrum with $S = 15$.

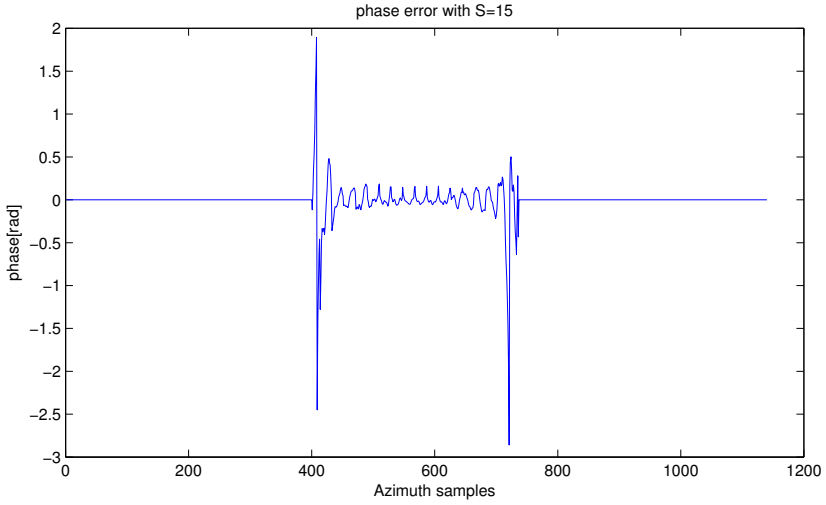

Figure 5.8: Phase error of the spectrum with $S = 15$.

In figure 5.6 can be seen that we have made an error in the final focused image and the phase error of figure 5.8 is not equal to zero near the target position. In this case we use a sub-sampling factor $S = 15$ too big and this brings us to make some errors in the final focused image. The results above are compared with the full back-projection algorithm results. The images obained with the full algorithm are those of figures 3.2 and 3.3.

Now we want to change the central carrier frequency of the SAR system to see the differences respect to the previous case. Now we have this system parameters:

Parameter	Symbol	Value
Wavelength	λ	0.5 $[m]$
Azimuth sampling	dx	0.5 $[m]$
Range sampling	dr	3 $[m]$
Antenna Length	L_a	4 $[m]$
Nominal distance to ground	R_0	3 $[km]$
Maximum subsamping	S_{max}	18.1142

Table 5.1: Table of system parameters

So now we have double the wavelength and so we have double the BT product, but we hold the same sampling interval dx. The first images are taken using a value of S equal to 19.

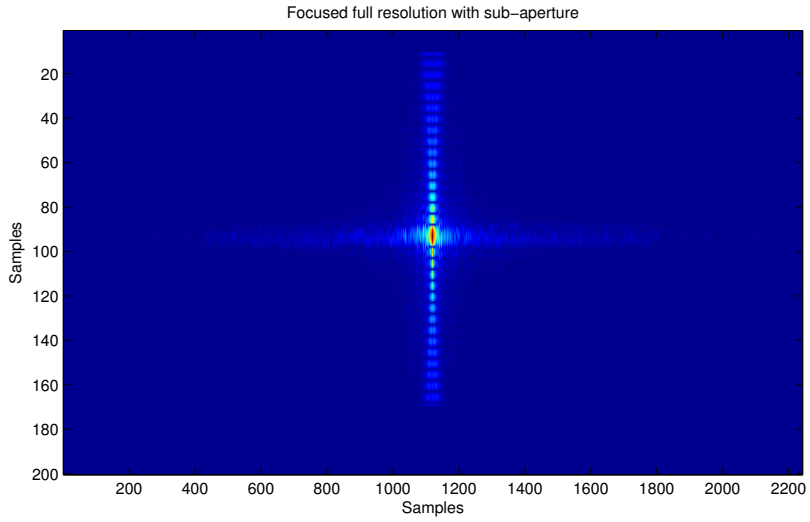

Figure 5.9: Final focused image with $S = 19$ and the system parameters are those of table 5.1.

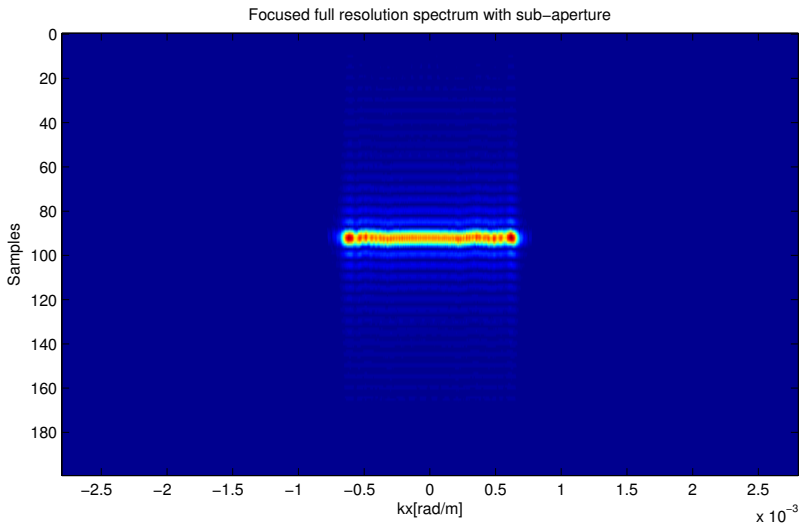

Figure 5.10: Final focused image spectrum with $S = 19$.

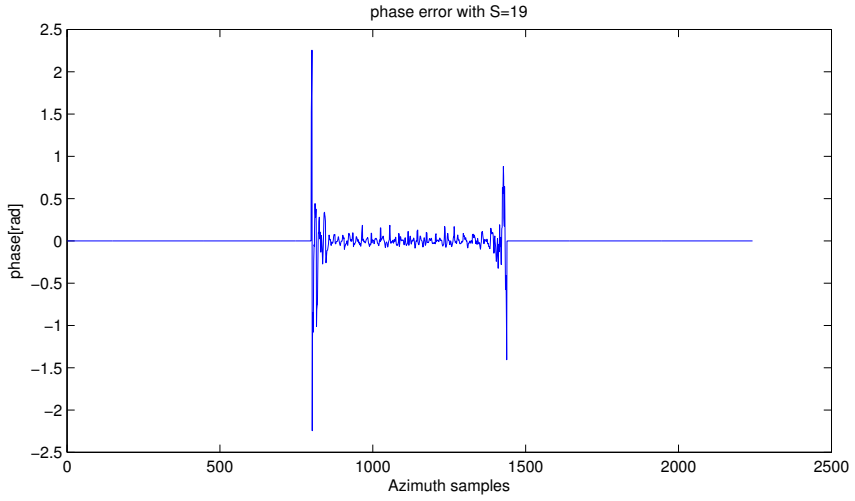

Figure 5.11: Phase error of the spectrum with $S = 19$.

The image focused with the full back-projection integral and its spectrum are shown in the next figures.

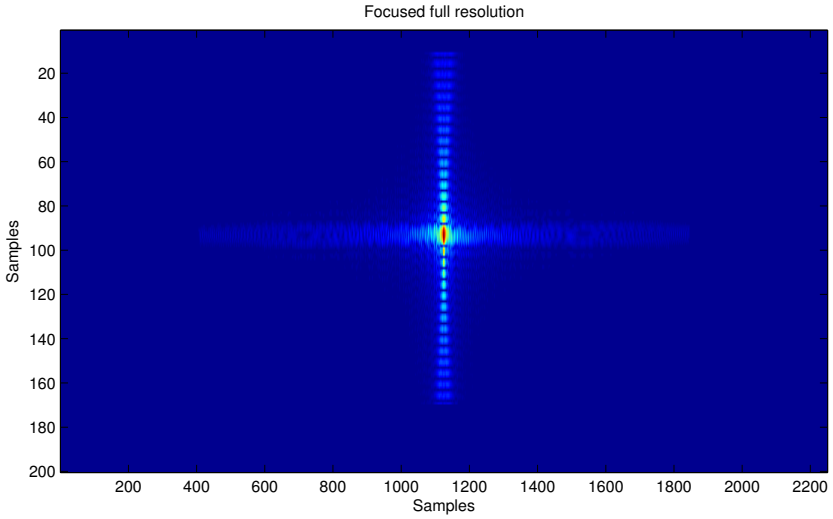

Figure 5.12: Final focused image with system parameters of table 5.1.

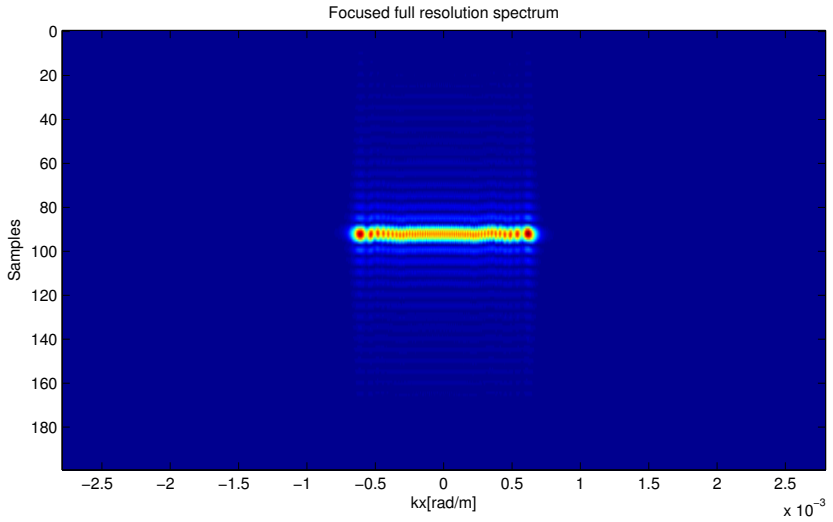

Figure 5.13: Final focused image spectrum.

Here we have used a value of S slightly higher than S_{max}. The phase error is quiet nosing at the center of the image, but the results are acceptable yet compared to those of figures 5.12 and 5.13. If we take a value of S bigger than S_{max} we make some errors in the final image as shown in the next figures.

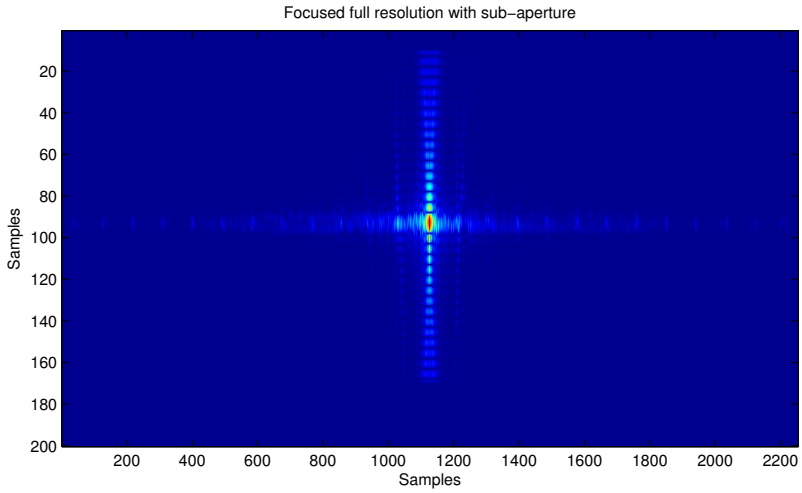

Figure 5.14: Final focused image with $S = 23$ and the system parameters are those of table 5.1.

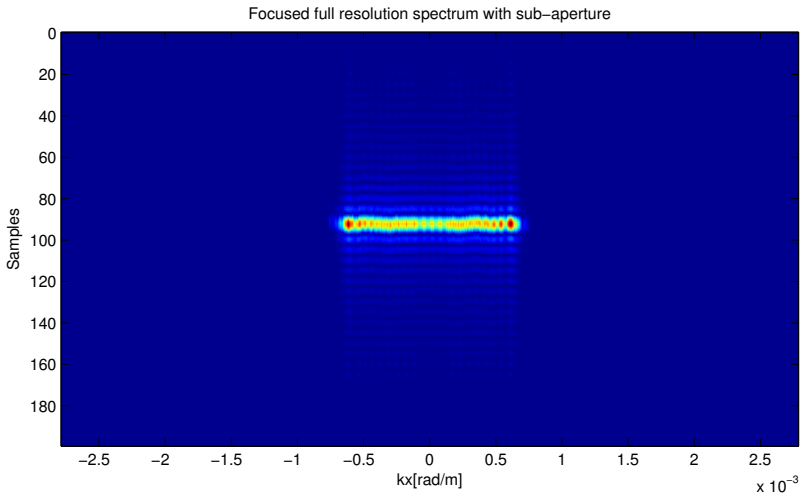

Figure 5.15: Final focused image spectrum with $S = 23$.

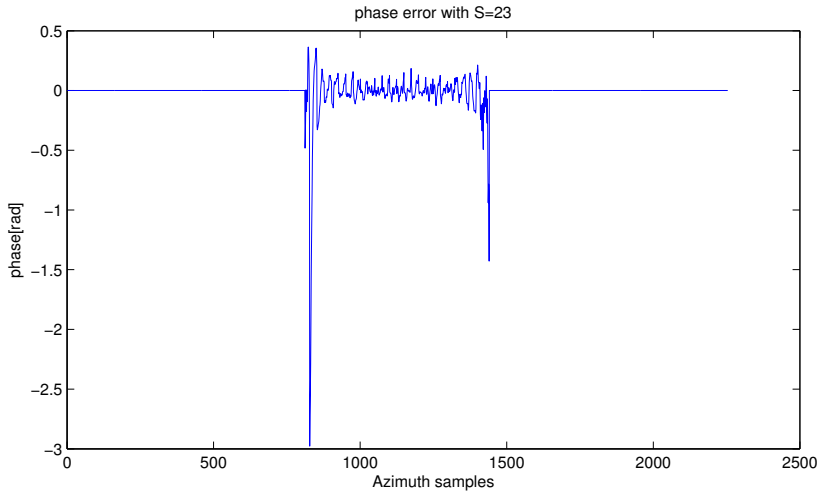

Figure 5.16: Phase error of the spectrum with $S = 23$.

5.3 Change the trajectory

Now we want to study the effect of the trajectory. We said that, due to the flight motion, the linear slope of the frequency components doesn't hold on for the raw data. During the focusing this phase term is corrected and so we aspect to obtain the same results as before even if we change the trajectory. Suppose to have a trajectory like that of figure 5.17 and the system SAR parameters are those of table 4.1 and $S = 11$.

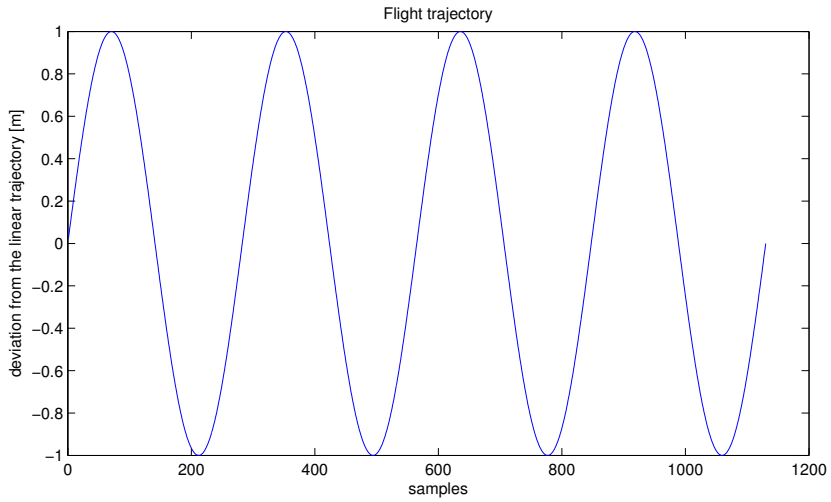

Figure 5.17: Fligth trajectory respect to the linear track centered on $y = 0$.

The raw data matrix and the raw data spectrum are shows in the nex figures.

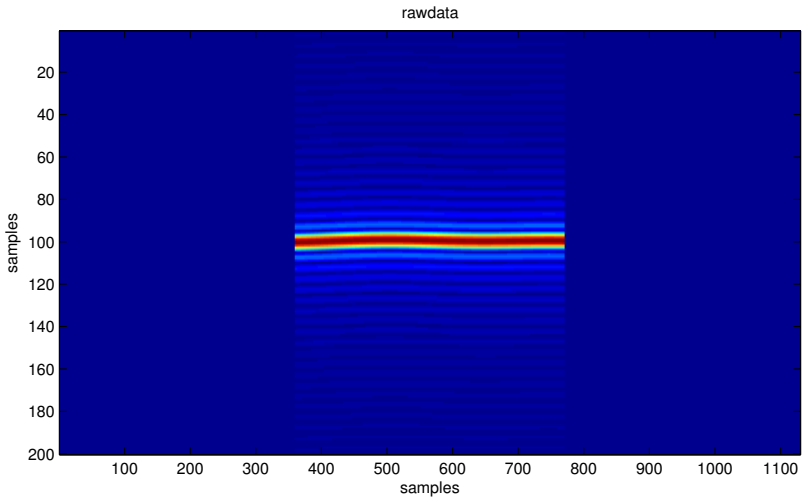

Figure 5.18: Rawdata matrix

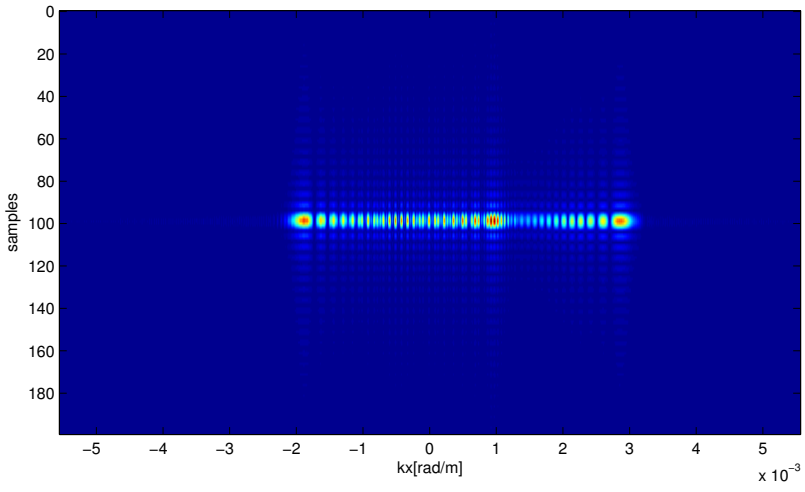

Figure 5.19: Rawdata matrix spectrum.

The final image and the final image spectrum are:

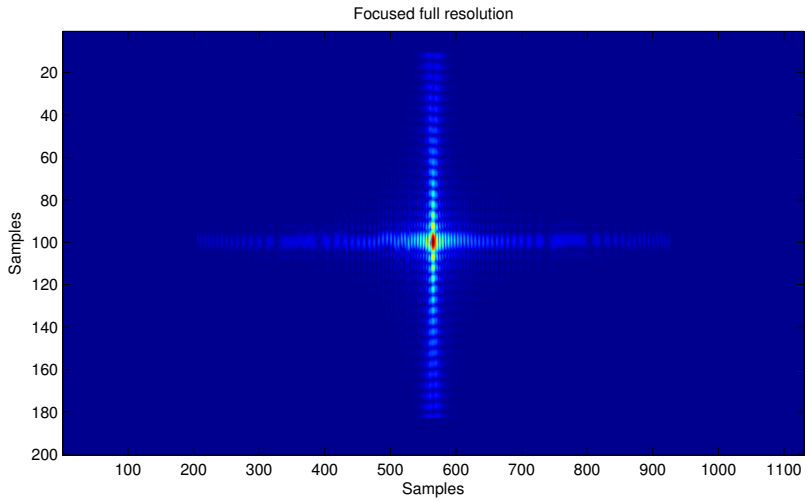

Figure 5.20: Focused full image, the phase due to the motion is corrected .

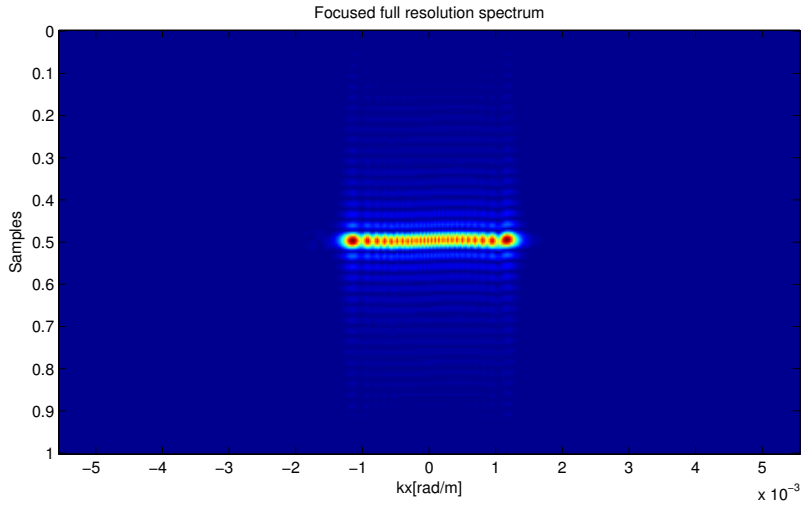

Figure 5.21: Focused full image spectrum.

Now we use our algorithm to focusing the data with $S = 11$ like for the image obtained in figure 5.3.

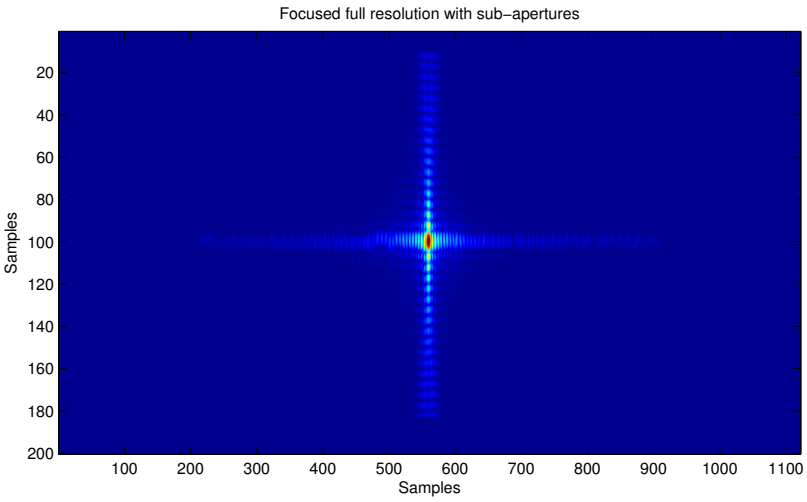

Figure 5.22: Zoomed final focused image with $S = 11$.

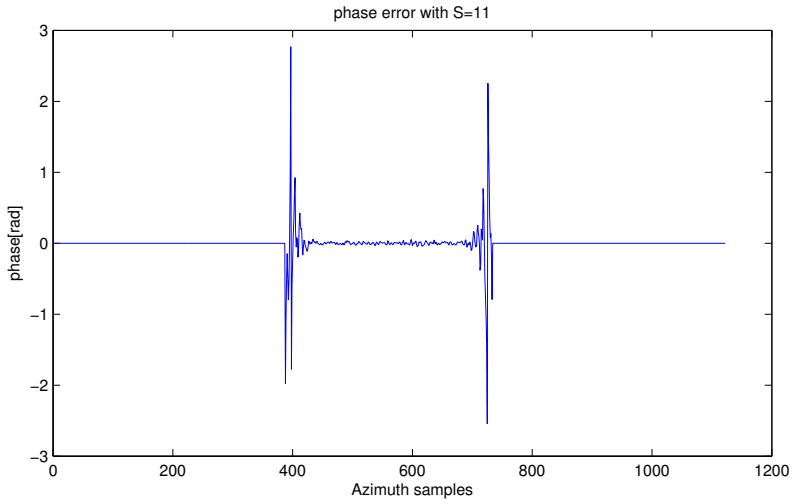

Figure 5.23: Phase error of the spectrum with $S = 11$.

Even if the rawdata and the rawdata spectrum are quiet different in figures 3.2 and 3.3 respect to those of figures 5.18 and 5.19 the final images 5.22 and 5.3 are quiet equal. This means that if we know the trajectory we can correct it without lose azimuth resolution.

Chapter 6

Conclusion

In this thesys we talk about the synthetic aperture radar data acquisition and then we explain a time-domain algorithm to process the rawdata matrix to get the final image.
We use a time domain method because it's very robust against the non linear trajectories of the airplain flights. The main drawback of this method is the computational bourden due to the large number of samples collected by the radar system.
In the time domain focusing algorithms the phase term due to the fligth trajectory is corrected in a general way and we don't have to derive some conditions only locally valid like in the Fourier Transform algorithms based.
To decrease the computational cost we derive a time domain method based on the divisions and subsamples of the whole synthetic aperture. In chapter four we describe a method to reconstruct the full resolution images combining the sub-apertures working on the spectrums. Thanks to the subsampling in the image azimuth points we have reduced the computational burden by a factor near the number of sub-apertures S.
We found the bounds of that algorithm based on the space-bandwidth product and, if we stay inside these limits, we demonstrate that we can obtain good results in term of phase error.
In chapter five we have established that this algorithm is very robust also in non-linear trajectory, that is the common case of the airplain SAR missions.
This work is a base on which can be achieved a fast and robust time domain algorithm for SAR focusing. An important feature on which can be work is the change of the coordinates systems as polar coordinates instead of the cartesian coordinates to improve the performance of this algorithm by reducing the phase range and so increasing the subsampling factor S.

Bibliography

[1] Andrea Monti Guarnieri. Introduction to RADAR.

[2] R.O. Harger. Synthetic aperture radar fundamentals and image processing. *EARSeL ADVANCES IN REMOTE SENSING*, 2(1):269–586, January 1993.

[3] David G. Messerschmitt John R. Barry, Edward A. Lee. *Digital Communication*. Kluwer Academics.

[4] Fabio Rocca. Elaborazione numerica dei segnali.

[5] L.M.H. Ulander, H. Hellsten, and G. Stenstrom. Synthetic-aperture radar processing using fast factorized back-projection. *Aerospace and Electronic Systems, IEEE Transactions on*, 39(3):760–776, July 2003.